Transport of *n*-paraffins in Zeolite T

Fernão D. Magalhães, Robert L. Laurence, and William Curtis Conner
Dept. of Chemical Engineering, University of Massachusetts at Amherst, Amherst, MA 01003

Mass transport of n-heptane, n-nonane, and n-dodecane in zeolite T was studied using a gravimetric uptake technique. The sigmoidal shape of the uptake curves indicated the existence of a nondiffusional resistance in the transport process. To compute the transport parameters, an approach based on the temporal moments of the uptake curves was developed. A model involving an external resistance dependent on the local slope of the sorption isotherm best represented the data. No evidence of the "window effect" reported by Gorring was found. The measured diffusivities decrease with chain length, while the activation energies remain essentially constant. Both resistances (diffusional and nondiffusional) depend strongly on lattice loading, and their relative contributions for the transport time change as saturation is approached.

Introduction

One of the most intriguing phenomena associated with mass transport in zeolites is the "window effect" reported by Gorring (1973) in a gravimetric study of diffusivity of linear paraffins in zeolite T. Despite the attention and discussion given to this effect in the literature (Froment and Bischoff, 1990; Wei, 1973), no work has been published confirming Gorring's data.

Here we report a study of the mass transport of some *n*-paraffins in zeolite T using gravimetric sorption/desorption. Investigation of the existence of the window effect was our original goal. However, evidence of nondiffusional mass transfer (surface barrier) prompted an unconventional analysis of the experimental data. Before initiating the description of our approach, we shall review briefly the published work concerning the two phenomena: the window effect and surface barriers.

Window effect

The diffusion coefficients measured by Gorring (shown in Figure 1) demonstrate the existence of a minimum for the diffusivity of *n*-octane, followed by a maximum for dodecane, the difference between the two extrema being of two orders of magnitude. In his explanation of this phenomenon, Gorring first recognized that diffusion in zeolite T (an intergrowth of offretite and erionite regions) is controlled by the small channels in the erionite regions. After analysis of the chain length of the paraffins and some geometric considerations, he concluded that molecules smaller than *n*-octane fit entirely inside erionite's cages. Inside the cage, the molecule resides in a deep potential well (the narrow eight membered rings—"windows"—that connect the cages give rise to a significant repulsion to the chain movement). The diffusivity decrease between C_3 and C_8 was attributed to molecular weight effects. Larger molecules, however, do not fit inside the cage, and have to extend through the eight-membered rings. Therefore, they are not "trapped" in the cage's potential well, and must have a larger diffusivity. The fraction of the molecular length located outside the cage increases between C_9 and C_{12}. This would explain the diffusivity increase in this interval. C_{12} extends entirely through a unit cell, between the extremes of the eight-membered rings. One may then think that dodecane corresponds to a critical point and molecular weight and steric effects may take over for larger molecules. Gorring also noted that the observed diffusivity dependence on the chain length can be used to justify the unexpected product distribution obtained from the catalytic cracking of *n*-C_{23} over *H*-erionite reported by Chen and coworkers (Chen et al., 1969).

Gorring's results were later discussed by Ruckenstein and Lee (1976). They summarized Gorring's intricate considerations in a more general, but still qualitative fashion. They considered a molecule moving along a linear periodic potential (associated to the succession of channels and cages in a zeolite pore). The period of this potential, L, coincides with the period of the zeolite's framework. A molecule with length equal to L (or an integer multiple of L) will assume a potential that is independent of its position along the one-dimen-

Correspondence concerning this article should be addressed to W. C. Conner.

sional pore. Since there are no energetic barriers to overcome, the diffusion process will show no activation energy. This molecule would then exhibit the faster diffusion rate. This would be the case of dodecane in the erionite system. Smaller and longer molecules will be subject to energetic potential barriers, and thus will have lower diffusivities. Ruckenstein and Lee termed this effect "resonant diffusion."

More recently, a quantitative approach was developed by Nitsche and Wei (1991). They described the diffusion of linear paraffins in erionite also as a one-dimensional process, in which the molecule (modeled as a rigid rod) moves along a periodic potential, which they have quantified by first specifying the interactions between the molecule's segments and the zeolite's framework. The energy barriers that the entire molecule must overcome can then be computed. As in the previous analysis, molecules with length multiple of the potential's period show zero activation energy. The authors in addition have adopted a Brownian motion model to describe the relationship between the diffusion coefficient and the periodic potential acting on the molecule. The results obtained fit Gorring's data relatively well.

It is intriguing that there are no reports of similar effects occurring in other systems. One would expect that frameworks characterized by periodic sequences of tight channels and relatively wide cages (like chabazite or 5A) would satisfy the conditions for the existence of such phenomena. The extensive work performed by Ruthven and coworkers on the diffusion of linear paraffins in zeolites 5A, silicalite and NaX (Ruthven and Eic, 1988; Vavlitis et al., 1981) shows no evidence of a window effect.

Surface barriers

Our sorption uptake curves show an unambiguous sigmoidal shape. This is typically associated with nondiffusional mass-transfer resistances. The hypothesis of surface barriers affecting the mass transport in some zeolite systems has been investigated to some extent in the last two decades.

Kondis and Dranoff (1971) obtained slightly sigmoidal uptake curves for adsorption and desorption of ethane in 4A zeolite. Bülow and coworkers also reported sigmoidal uptake curves for sorption of *n*-hexane in MgA (Bülow et al., 1980) and *n*-decane in NaMgA (Bülow et al., 1982). These observations were attributed to a particle surface resistance. In particular, there is evidence that the development of this resistance in zeolite A systems is related to the severity of the hydrothermal pretreatment of the samples (Bülow et al., 1980, 1982, 1985; Kondis and Dranoff, 1971). It has been suggested that this is due to an effect similar to the one observed in zeolite HY (Breck, 1974a): Al is removed from the framework by hydrolysis at high temperature, and, consequently, the frameworks' unit cell dimensions are reduced, giving rise to narrower pore openings. Additional evidence relative to the existence and nature of surface barriers in zeolite 5A systems has been provided by NMR experiments (e.g., Kärger et al., 1981, 1987, 1988).

In addition to this framework-structure related resistance, other possibilities have been discussed in the literature (Bülow, 1991). We list here the hypotheses we find pertinent:

(i) Conformational barrier (Bülow et al., 1980). In order to diffuse into the crystal, a molecule may have to undergo a change in conformation. In the case of a linear paraffin diffusing into a small channel system like 5A, the molecule must pass from a coiled conformation (the more stable in the gas phase) into a more elongated one, through rotations of the chain segments. The activation step associated with this transformation may induce an extracrystalline transport barrier. Experimental evidence of this phenomenon is not conclusive.

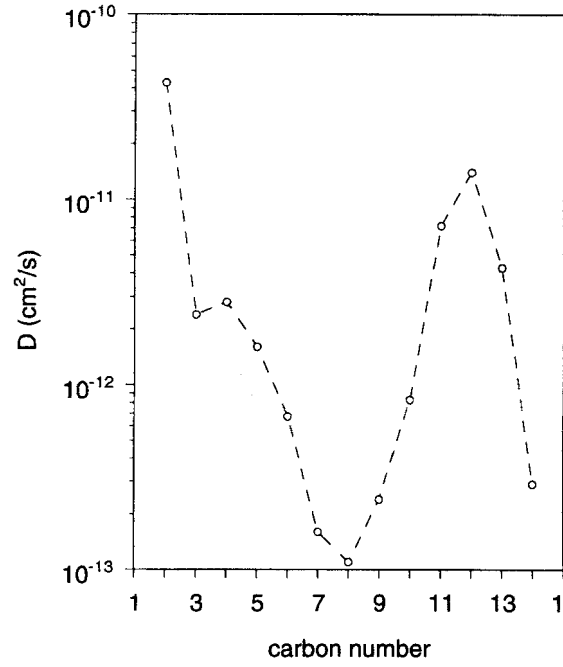

Figure 1. Diffusivities of *n*-paraffins in zeolite T at 300°C reported by Gorring.

The carbon number refers to the number of carbon atoms in the paraffin chain.

(ii) Evaporation barrier (Barrer, 1987). During desorption, molecules must acquire enough energy in order to escape the interactions with the framework. If this desorption energy is higher than the activation energy for intracrystalline diffusion, an evaporation barrier is present at the crystal surface. There is no experimental evidence of this effect (Kärger and Ruthven, 1989).

(iii) Thermal barrier (Bülow and Struve, 1984). If the heat of adsorption is not efficiently dissipated from the crystal interface, the local temperature may increase, causing the sorbate concentration to decrease and thus delaying the adsorption uptake. It was shown that this effect is significant in the adsorption of benzene by NaX zeolite.

(iv) Nonequilibrium barrier (Micke et al., 1994). Adsorption at the surface may not be an instantaneous equilibrium process. The particular kinetics of the process may give rise to an apparent surface barrier. A model assuming Langmuir kinetics at the crystal surface did fit the experimental results well for the system *p*-ethyl-toluene–ZSM-5.

Theory

Mathematical model

The structural relationship between the synthetic zeolite Linde T and the natural zeolites offretite and erionite was

elucidated by Bennett and Gard (1967). They proposed that zeolite T is a disordered intergrowth of erionite and offretite, the latter being the predominant phase. The erionite regions form thin layers within the offretite matrix. They may be viewed as defects in the framework. Fault-free offretite is a typical large-pore zeolite like Linde X or Y. Straight pores, formed by circular 12-membered ring apertures [6.7 Å in diameter (Meier and Olson, 1992], establish a favorable route for diffusion of both linear and cyclical molecules. The erionite intergrowths, as noted by Gorring (1973) and Chen (Chen, 1972), are bottlenecks in offretite's large-pore framework. Diffusion through the erionite regions is possible only through 8-membered rings [3.6×5.1 Å in diameter (Meier and Olson, 1992)] in a zig-zag path. Only linear paraffins are able to pass through apertures with such small dimensions (Barrer and Peterson, 1964; Xiao and Wei, 1992). This picture suggests that intracrystalline transport of a linear paraffin in zeolite T can be described by a simple two-resistances-in-series model (Nitsche and Wei, 1991):

$$\frac{1}{D_z} = \frac{\phi_{\text{eri}}}{D_{\text{eri}}} + \frac{1-\phi_{\text{eri}}}{D_{\text{off}}}. \tag{1}$$

One expects the erionite's resistance term to be dominant. The diffusivity of heptane in a 8-membered ring system (such as zeolite 5A) is four orders of magnitude lower than in a 12-membered system (such as zeolite X) (Kärger and Ruthven, 1992). The total volume fraction of erionite in the crystal, ϕ_{eri}, is typically quite small (2–5%) (Chen, 1972; Gorring, 1973). This may affect the relative importance of the erionite's resistance term in Eq. 1.

We shall assume that the intracrystalline transport can be described by the diffusion equation. The transport is characterized by an effective diffusion coefficient, D_z, describing diffusion in the two constituent regions. The material balance takes the form:

$$D_z\left(\frac{\partial^2 \bar{q}(r,t)}{\partial r^2} + \frac{2}{r}\frac{\partial \bar{q}(r,t)}{\partial r}\right) = \frac{\partial \bar{q}(r,t)}{\partial t} \tag{2}$$

with boundary conditions:

$$t = 0 \Rightarrow \bar{q}(r,0) = 0 \tag{3}$$

$$r = 0 \Rightarrow \left.\frac{\partial \bar{q}(r,t)}{\partial r}\right|_{r=0} = 0 \tag{4}$$

$$r = R \Rightarrow \bar{q}(R,t) = K\bar{C}_i(t), \tag{5}$$

where $\bar{q}$ and $\bar{C}_i$ are displacement variables:

$$\bar{q}(r,t) = q(r,t) - q(r,0) \tag{6}$$

$$\bar{C}_i(t) = C_i(t) - C_i(0). \tag{7}$$

The effective diffusivity D_z is assumed constant over the concentration range corresponding to each adsorption (or desorption) step. Furthermore, we shall assume that K, in Eq. 5, may be approximated by the local slope of the adsorption isotherm:

$$K(\theta_m) = \frac{\bar{q}(R,t)}{\bar{C}_i(t)} \sim \left.\frac{d(q_{\text{eq}})}{d(C_b,\text{eq})}\right|_{\theta_m}, \tag{8}$$

where θ_m is the mean fractional occupancy for the corresponding step:

$$\theta_m = \frac{1}{2}\frac{m_0 + m_\infty}{m_{\max}} \tag{9}$$

(from here on, the subscript will be omitted from θ_m). The approximation in Eq. 8 is valid only if the step is sufficiently small, enabling the assumption that the isotherm may be assumed as linear over that concentration range. This can be critical at intermediate occupancies, where the isotherm shows the greatest curvature.

Our measured transient uptake curves show a distinct sigmoidal shape. In order to account for this, two other features were added to the model: external resistance to mass transfer, and a nonideal step in the bulk-gas adsorbate concentration. The external resistance is considered in two alternative formulations: (a) the resistance is located in the external gas–phase; and (b) the resistance is located in the particle's surface. The resistance in (a) may be associated with a stagnant gas–phase film surrounding the particle or with an ineffective gas–phase mixing between the free stream and the particle bed. The specific nature of these resistances will not be detailed any further. It is assumed that they can be expressed in terms of mass-transfer coefficients (k_f and k_s, respectively). The corresponding mass balances are

$$D_z\left.\frac{\partial \bar{q}(r,t)}{\partial r}\right|_{r=R} = k_f[\bar{C}_b(t) - \bar{C}_i(t)] \tag{10}$$

and

$$D_z\left.\frac{\partial \bar{q}(r,t)}{\partial r}\right|_{r=R} = k_s[\bar{q}_i(t) - \bar{q}(R,t)], \tag{11}$$

where

$$\bar{C}_b(t) = C_b(t) - C_b(0) \tag{12}$$

$$\bar{q}_i(t) = q_i(t) - q_i(0). \tag{13}$$

The subscript i denotes concentration at the gas-phase/particle-surface interface. Notice that when considering case (b) (Eq. 11), boundary condition 5 takes the form:

$$r = R \Rightarrow \bar{q}_i(R,t) = K\bar{C}_b(t). \tag{14}$$

Finally, we allow the bulk gas phase concentration, $\bar{C}_b$, to be time-dependent. This should account to such effects as response time of the mass-flow controllers, mixing, axial dispersion, and parabolic velocity profile. This dependence is probably sigmoidal in shape and can be approximated by the following expression:

$$\bar{C}_b(t) = H(t-\tau_{c1})\left\{1 - \exp\left[-\frac{1}{\tau_{c2}}(t-\tau_{c1})\right]\right\}\Delta C_b. \tag{15}$$

The set of three equations that defines the problem (Eqs. 2, 10, or 11, and 15) can be solved after transformation into the Laplace domain. The intracrystalline mass balance becomes (the $\sim$ over the variables designates their Laplace transform):

$$D_z\left(\frac{\partial^2\tilde{q}(r,s)}{\partial r^2}+\frac{2}{r}\frac{\partial\tilde{q}(r,s)}{\partial r}\right)=s\tilde{q}(r,s) \tag{16}$$

$$r=0\Rightarrow\left.\frac{\partial\tilde{q}(r,s)}{\partial r}\right|_{r=0}=0 \tag{17}$$

$$r=R\Rightarrow\tilde{q}(R,s)=K\tilde{C}_i(s)\quad\text{or}\quad\tilde{q}(R,s)=K\tilde{C}_b(s). \tag{18}$$

The external resistance

$$D_z\left.\frac{\partial\tilde{q}(r,s)}{\partial r}\right|_{r=R}=k_f[\tilde{C}_b(s)-\tilde{C}_i(s)] \tag{19}$$

or

$$D_z\left.\frac{\partial\tilde{q}(r,s)}{\partial r}\right|_{r=R}=k_s[\tilde{q}_i(s)-\tilde{q}(R,s)]. \tag{20}$$

And the gas-phase adsorbate concentration

$$\tilde{C}_b(s)=\frac{\Delta C_b\exp(-\tau_{c1}s)}{s(\tau_{c2}s+1)}. \tag{21}$$

Equation 16 is a modified spherical Bessel's equation, whose solution may be expressed in terms of hyperbolic functions (Abramowitz and Stegun, 1965). The final expression of $\tilde{q}(r,s)$ is lengthy and is not presented here.

The mean concentration inside the particle, $\bar{Q}(t)$, can be obtained from the concentration profile $\bar{q}(r,t)$ using the following relationship:

$$\frac{4}{3}\pi R^3\frac{d\bar{Q}(t)}{dt}=4\pi R^2D_z\left.\frac{\partial\bar{q}(r,t)}{\partial r}\right|_{r=R}, \tag{22}$$

or, in the Laplace domain:

$$\tilde{Q}(s)=\frac{1}{s}\frac{3}{R}D_z\left.\frac{\partial\tilde{q}(r,s)}{\partial r}\right|_{r=R}. \tag{23}$$

The resulting expression is, in terms of fractional uptake, $f(t)=(m-m_0)/(m_\infty-m_0)=\bar{Q}(t)/(K\Delta C_b)$:

$$\tilde{f}(s)=\frac{3\exp(-\tau_{c1}s)}{(\tau_{c2}s+1)s\sqrt{s\tau_{\text{diff}}}\left\{\left[\coth\left(\sqrt{s\tau_{\text{diff}}}\right)-\left(\sqrt{s\tau_{\text{diff}}}\right)^{-1}\right]^{-1}+\frac{\sqrt{s\tau_{\text{diff}}}}{Bi_m}\right\}}, \tag{24}$$

where τ_{diff} is the time constant for intracrystalline diffusion:

$$\tau_{\text{diff}}=\frac{R^2}{D_z}, \tag{25}$$

Bi_m is the Biot number for mass transfer. This is defined as

$$Bi_m=\frac{k_fR}{D_zK} \tag{26}$$

when the external mass-transfer resistance is associated with a gas-phase resistance (Eq. 10); or as

$$Bi_m=\frac{k_sR}{D_z} \tag{27}$$

when the resistance is at the particle's external surface (Eq. 11). Bi_m is related to the ratio between the intracrystalline diffusion and external resistance time constants.

Analytical solutions in the time domain were obtained by Crank for the separate problems of intracrystalline diffusion with time-dependent bulk gas phase concentration and intracrystalline diffusion with external gas-film resistance (Crank, 1975).

Fractional uptake vs. time solutions can be obtained by numerically inverting Eq. 24 into the time domain. IMSL routine INLAP was used for this purpose. Some uptake curves are shown in Figure 2. Curve (1), obtained for $Bi_m\to\infty$, corresponds to intracrystalline diffusion control. In this case, the first portion of the curve, for small times, is linear with $t^{1/2}$. From the corresponding slope one can compute directly the diffusion coefficient, D_z, (Crank, 1975). This fact (usually referred to as "$\sqrt{t}$ law") is the basis for the traditional treatment of transient uptake experiments. This does not hold, however, when a significant external resistance or nonideal gas-bulk concentration step is present, since the uptake curves become increasingly sigmoidal in shape as the Biot number decreases, or as τ_{c1} and τ_{c2} increase.

It is also interesting to analyze the limiting case of external resistance control ($D_z\to\infty$). The only necessary material balance is (for gas-phase resistance)

$$\frac{d\bar{q}}{dt}=\frac{3k_f}{R}(\bar{C}_b-\bar{C}_i)=\frac{3k_f}{R}\left(\frac{\bar{q}_\infty}{K}-\frac{\bar{q}}{K}\right). \tag{28}$$

This can be solved, in terms of the fractional uptake, f, to yield

$$\ln(1-f)=-\frac{3k_f}{RK}t. \tag{29}$$

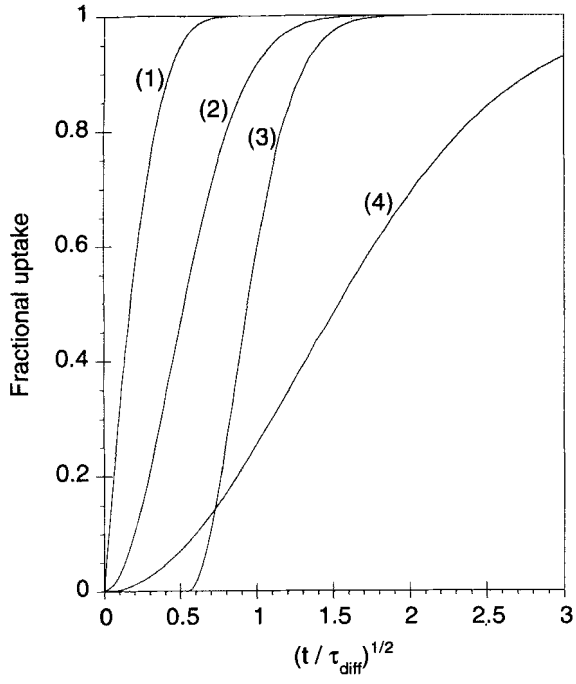

Figure 2. Uptake curves obtained by numerical inversion of Eq. 24.

The numbers on the curves correspond to the following parameters: (1) $Bi_m \to \infty$, $\tau_{c1}/\tau_{diff} = 0$, $\tau_{c2}/\tau_{diff} = 0$; (2) $Bi_m = 1$, $\tau_{c1}/\tau_{diff} = 0$, $\tau_{c2}/\tau_{diff} = 0$; (3) $Bi_m = 1$, $\tau_{c1}/\tau_{diff} = 0.3$, $\tau_{c2}/\tau_{diff} = 0.3$; (4) $Bi_m = 0.1$, $\tau_{c1}/\tau_{diff} = 0$, $\tau_{c2}/\tau_{diff} = 0$.

When the resistance is at the surface of the crystal we would have

$$\ln(1-f) = -\frac{3k_s}{R}t. \tag{30}$$

This scenario is a particular case of the complete model, since, when $D_z \to \infty$, Eq. 24 becomes the Laplace transform of Eq. 28 (or 29, depending on the definition of Bi_m). Both Eqs. 29 and 30 show a linear time-dependence of $\ln(1-f)$. This result is commonly described as the criterion for identifying an external gas film or surface resistance control (Kärger and Ruthven, 1992a; Riekert, 1989). However, this is not always an indication that external transport is the dominant resistance in the mass-transfer process. To show this, plots of $\log(1-f)$ vs. time are shown on Figure 3, for different values of Bi_m. Curves (3) and (4) are both essentially linear. However, curve (3), with $Bi_m = 1$, does not yet correspond to pure external resistance control. This can be seen by comparing curve (3) to the plot of Eq. 28 or 29—dashed line on Figure 3—using the relationship

$$\frac{k_f}{RK} = \frac{Bi_m}{\tau_{diff}} \quad \text{or} \quad \frac{k_s}{R} = \frac{Bi_m}{\tau_{diff}}. \tag{31}$$

The two plots do not coincide. Only for a smaller value of Bi_m (curve (4)) do both models coincide.

When the transport process is diffusion-controlled (curve (1) in Figure 3), the long-time portion of the curve may be approximated by Kärger and Ruthven (1992b).

$$\ln(1-f) = \ln\left(\frac{6}{\pi^2}\right) - \frac{D_z\pi^2}{R^2}t. \tag{32}$$

Thus, D_z can be estimated from the slope of the linear region of the curve (dotted–dashed line in Figure 3).

Temporal moments

The use of the statistical moments obtained from the transient uptake data in the analysis of transport properties was first suggested by Kocirik and Zikánová (Kocirik and Zikánová, 1970, 1974). Their objective was to study the individual contributions to the transport process of the macro- and microporous regions in a bidisperse material. Dubinin and coworkers (Dubinin et al., 1975) developed the method further, for biporous adsorbents. Kärger and coworkers (Kärger et al., 1982) suggested using the temporal moments for samples of varying particle radius to identify the limiting process in the sorption kinetics.

The moments are computed in relation to the first time

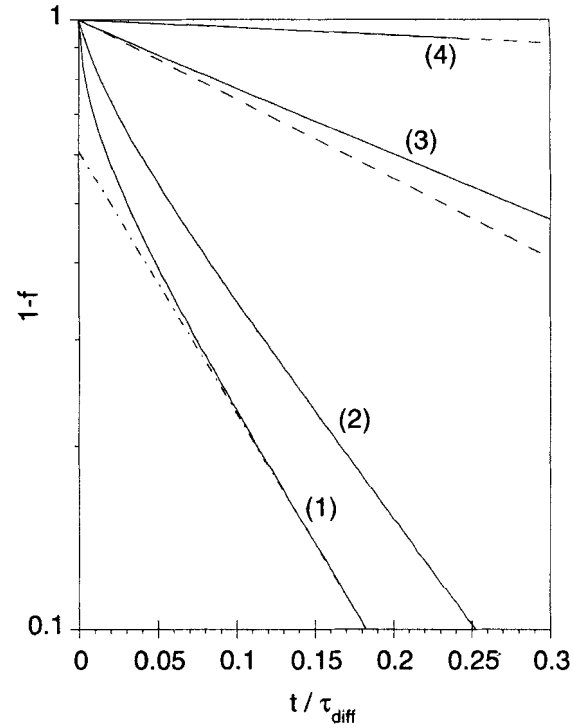

Figure 3. Uptake curves obtained by numerical inversion of Eq. 24.

$\tau_{c1} = \tau_{c2} = 0$ for all curves. The numbers on the curves correspond to the following values of Bi_m: (1) $Bi_m \to \infty$; (2) $Bi_m = 10$; (3) $Bi_m = 1$; (4) $Bi_m = 0.1$. The dashed lines are plots of $\ln(1-f) = -3t\ (Bi_m/\tau_{diff})$ for the conditions of curves (3) and (4). The dashed–dotted line is the plot of Eq. 32 for the conditions of curve (1).

derivative of the fractional uptake, $f(t)$. An analytical expression for the kth moment can be obtained from the Laplace transform $\tilde{f}(s)$ (see Eq. 24):

$$M_k = \int_0^\infty t^k \frac{df}{dt} dt = (-1)^k \lim_{s \to 0} \frac{d^k}{ds^k} \left(L\left\{ \frac{df}{dt} \right\} \right)$$

$$= (-1)^k \lim_{s \to 0} \frac{d^k}{ds^k} (s\tilde{f}(s)). \quad (33)$$

This way, the following expressions can be derived for the first and second moments:

$$M_1 = (\tau_{c1} + \tau_{c2}) + \frac{\tau_{\text{diff}}}{15} + \frac{\tau_{\text{diff}}}{3Bi_m} \quad (34)$$

$$\frac{M_2}{2} = \left({\tau_{c1}}^2 + \tau_{c1}\tau_{c2} + \frac{{T_{c2}}^2}{2} \right) + \tau_{\text{diff}}(\tau_{c1} + \tau_{c1}) \left(\frac{\tau_{\text{diff}}}{15} + \frac{\tau_{\text{diff}}}{3Bi_m} \right)$$

$$+ \tau_{\text{diff}}^2 \left(\frac{2}{315} + \frac{2}{45Bi_m} + \frac{1}{9Bi_m^2} \right). \quad (35)$$

Equation 34, with $(\tau_{c1} + \tau_{c2}) = 0$, is equivalent to the expression derived by Kärger for the mean intracrystalline life time in a NMR tracer desorption experiment (Kärger, 1982).

In order to compute the moments from experimental data, one does not have to evaluate the time derivatives, since it can be shown that

$$M_k = k \int_0^\infty t^{k-1} [1 - f(t)] dt. \quad (36)$$

Note that the first moment is simply the area under the $1 - f(t)$ curve.

Parameter fitting in the Fourier domain

The initial estimates of the model's parameters (τ_{diff}, Bi_m, τ_{c1}, τ_{c2}) obtained from the experimental moments can, in principle, be improved using the Fourier domain-fitting technique. This technique has been applied successfully to the estimation of diffusion coefficients in a two-parameter model of chromatographic column with a polymer-coated capillary (Arnould and Laurence, 1989). The Fourier transform of the model can be obtained from Eq. 24 since

$$\hat{g}(k) = \frac{1}{t_\infty} \int_0^{t_\infty} g(t) \exp\left(-\frac{i\pi kt}{t_\infty} \right) dt = \frac{1}{t_\infty} \tilde{g}(s)$$

$$\text{with} \quad s = \frac{i\pi k}{t_\infty}, \quad (37)$$

where:

$$g(t) = 1 - f(t) \quad \text{and} \quad \tilde{g}(s) = L\{g(t)\}$$

$$= \left(\frac{1}{s} - \tilde{f}(s) \right). \quad (38)$$

The Fourier transform of the experimental uptake curve (more precisely, of $1 - f(t)$) is first computed, and then the difference between this and the theoretical transform minimized. This optimization is based on a least-squares criterion, since, according to Parseval's theorem, this criterion is equivalent in the time and Fourier domains. The objective function is then

$$F_{\text{obj}} = \int_0^\infty \left\{ [\text{Re}_{\text{exp}}(\omega) - \text{Re}_{\text{theo}}(\omega)]^2 \right.$$

$$\left. + [\text{Im}_{\text{exp}}(\omega) - \text{Im}_{\text{theo}}(\omega)]^2 \right\} d\omega, \quad (39)$$

where $\text{Re}(\omega)$ and $\text{Im}(\omega)$ are, respectively, the real and imaginary parts of the experimental or theoretical transforms. The parameter values computed from the statistical moments should be used as initial estimates. A modified Levenberg–Marquardt algorithm (IMSL routine BCLSF) was used for the fitting.

This problem shows, however, some particular features that seriously restrict the applicability of the technique. This is exemplified in Figure 4. A "true solution" corresponding to $\tau_{\text{diff}} = 100$, $Bi_m = 1$, and $\tau_{c1} = \tau_{c2} = 0$ was assumed. The objective function, F_{obj}, was then mapped for different values of the optimization parameters τ_{diff} and Bi_m (τ_{c1} and τ_{c2} were kept constant to simplify the analysis). F_{obj} is zero for the true solution and greater than zero elsewhere. In an ideal problem, the optimization surface would be a sharply defined well converging to the true solution (the absolute minimum). Figure 4 indicates that our problem is far from ideal. The response surface forms a "canyon." Its floor is relatively wide and has a very flat gradient toward the true solution. The

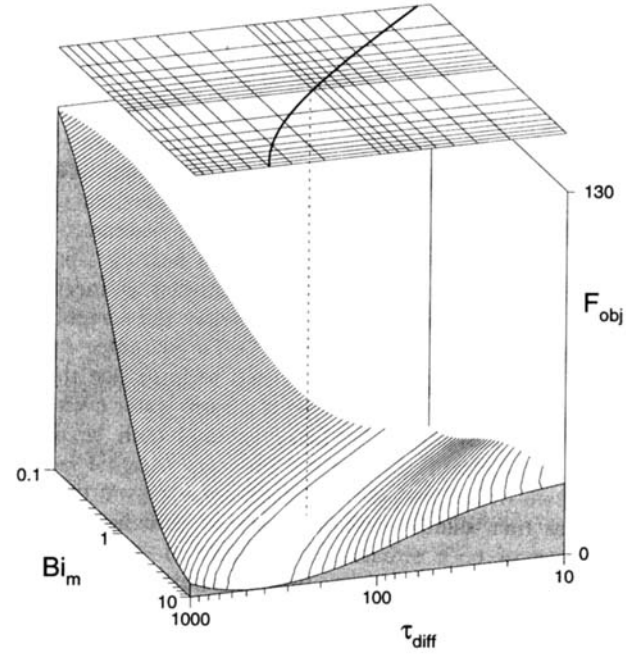

Figure 4. Optimization surface for the "true solution": $\tau_{\text{diff}} = 100$ s, $Bi_m = 1$, and $\tau_{c1} = \tau_{c2} = 0$ s.

Curve on the upper graph is defined by Eq. 34 with $M_1 = 40$ s and $\tau_{c1} = \tau_{c2} = 0$ s.

consequences are obvious: noisy experimental data cause the floor of the canyon to be unavoidably uneven, creating local minima. Finding the "true solution" becomes practically impossible. More optimization parameters make the task even more difficult.

The canyon's base, projected on the $\tau_{diff} - Bi_m$ plane, appears to follow Eq. 34 with M_1 equal to the first moment of the true solution (40 s) (see curve on the upper graph of Figure 4). An infinite set of values of τ_{diff} and Bi_m, correlated by Eq. 34, generate uptake curves with the same first moment and an almost identical image in the Fourier domain as the true solution.

The difficulties predicted by these observations were confirmed when working with experimental data. Depending on the initial estimates, numerous sets of parameters can be obtained from the fitting of a single uptake curve, and it was impossible to identify the true optimum solution. Parameter estimation in the Fourier domain is therefore essentially useless in the analysis of this problem.

Experimental Studies

Material

The zeolite T samples used in this work were prepared by A. W. Peters at W. R. Grace. The final composition was similar to Gorring's: alumina 16.0%, silica 70.5%, potassium 13.3%, sodium 0.2%.

Electron micrographs revealed that the zeolite particles had an ellipsoidal shape (about 1.6 μm in length and 0.8 μm in width). An average equivalent sphere diameter of 1.13 μm was assumed.

Prior to use, the samples were calcined in air at 450°C for 24 h and outgassed at 400°C and 10^{-5} torr for 12 h. Heating rates were kept low to avoid possible thermal stress effects on the framework.

Apparatus

The experimental setup is shown in Figure 5. A Cahn 2000 electrobalance was used for the weight measurements. The sample (20 to 30 mg) was placed in an aluminum weighing pan (~ 1 cm in diameter) inside a vertical glass column (~ 2.1 cm in diameter). Helium (the carrier gas) was introduced from below. The glass column was wrapped in heating tape and insulated. A Eurotherm temperature controller, connected to a thermocouple located immediately below the sample pan, regulated the temperature within 1°C. To guarantee saturation, two bubblers in series were used to introduce the adsorbate. Molecular sieve was used to adsorb water eventually dissolved in the liquid. A Haake thermal bath circulated heating/cooling fluid through the bubblers' external jackets. The stream of helium plus adsorbate coming from the bubblers was then diluted with a stream of pure helium. The flow rates of both streams were regulated by two Tylan mass-flow controllers. Setting the temperature in the bubblers and the ratio between the two gas streams' flow rates allowed control of the adsorbate concentration in the gas over the sample. To guarantee saturation of the bubblers stream, this flow rate was never greater than to 20 cm^3/min. The total gas flow rate going through the sample was always 100 cm^3/min.

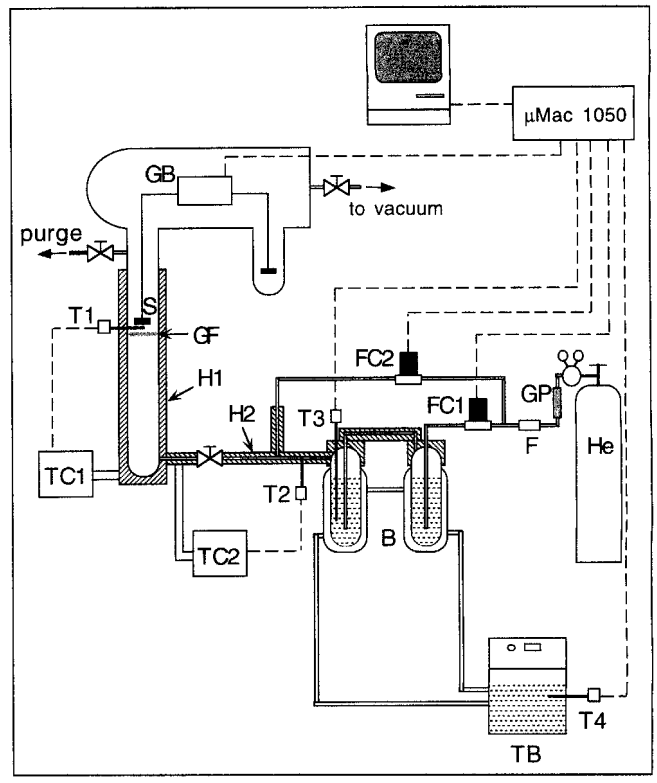

Figure 5. Experimental apparatus.

B—jacketed sorbate bubblers; F—filter; FC1, FC2—mass-flow controllers; GB—microgravimetric balance; GF—glass frit; H1, H2—heated regions; GP—gas purifier; T1, T2, T3, T4—thermocouples; TB—thermostatic bath; TC1, TC2—temperature controllers; S—sample pan.

Data acquisition was performed with an Azonix μMac 1050 unit connected to a Macintosh SE computer. Besides the transient weight measurements, the output and setpoints of the mass-flow controllers were also monitored.

Results and Discussion

n-Heptane

Isotherms. The sorption isotherms were obtained gravimetrically at three different temperatures (200, 250 and 300°C). These are shown in Figure 6. Since an explicit mathematical expression of the local slope of the isotherm, K, is necessary in the analysis of the transient uptake data, we tried to fit the data with simple equations for the isotherms. The best results were obtained by adding an interaction factor, β, to the Langmuir isotherm (Barrer, 1971):

$$p = \frac{\theta e^{\beta\theta}}{\alpha(1-\theta)}. \tag{40}$$

The parameter β can be interpreted as an interaction parameter: $\beta > 0$ implies repulsion between adsorbed molecules and $\beta < 0$ attraction. Equation 40 becomes the Langmuir isotherm when $\beta = 0$. We are not, however, concerned with a detailed analysis of the physical significance or accuracy of this model. As mentioned before, our only purpose is to obtain a simple analytical expression for K. This has the form:

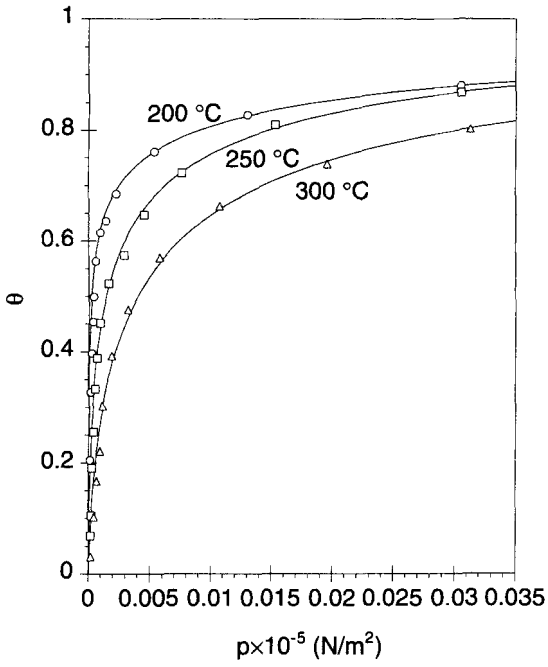

Figure 6. Isotherms for *n*-heptane sorption.

The curves correspond to the fits of Eq. 40 to the experimental data.

$$K(\theta) \sim \left.\frac{d(q_{eq})}{d(C_{b,eq})}\right|_{\theta} = \left(\frac{R_g T d_z m_{max}}{M_w m_{sample}}\right)\frac{d\theta}{dp}$$

$$= \left(\frac{R_g T d_z m_{max}}{M_w m_{sample}}\right)\frac{\alpha(1-\theta)^2}{e^{\beta\theta}(1+\beta\theta-\beta\theta^2)}. \quad (41)$$

A value of d_z (the framework density) = 1.50 g/cm^3 for zeolite T was obtained from Breck (1974b).

The values computed for parameters α and β are shown in Table 1.

Transient Mass Transfer. Each adsorption (or desorption) step was assumed isothermal, given the use of helium as carrier gas and the small amounts of sample employed. Furthermore, no significant change in the uptake data was detected by changing sample size.

One important aspect in these experiments is the size of the change in concentration, the step size. The change in adsorbate loading in each adsorption or desorption step should be small enough to guarantee the validity of the assumptions of constant local diffusivity and local isotherm linearity. If the step is too small, though, the baseline noise may affect the measurements. One can usually find the correct operation conditions by successively decreasing the step size until the uptake curves become essentially invariant. Also, agreement between adsorption and desorption curves can be used as a criterion. Garg and Ruthven (1972) have shown that, in a system where intracrystalline diffusion is concentration-dependent, adsorption and desorption curves will show an apparent diffusion coefficient higher than the true value. The discrepancy is stronger for the adsorption curves, and increases drastically with increasing step size. The magnitude of this effect should depend on the particular type of the isotherm. In general, we found that consistency between adsorption and desorption curves could be obtained with step changes in the sorbed amount not greater than about 8% of the maximum loading.

Table 1. Parameters α and β Obtained from Fitting Eq. 40 to Experimental Sorption Isotherms of *n*-Heptane

Temp. °C	α (N/m^2)$^{-1}$	β
200	1.82	7.52
250	3.41×10^{-2}	3.16
300	3.89×10^{-3}	1.46

A mass spectrometry analysis of the effluent during desorption showed no evidence of hydrocarbon cracking at the higher temperatures. The good reproducibility of the measurements and visual inspection of the samples after use indicated that coking was not significant.

The analysis of the transient data was based on the temporal moments of the uptake curves. The first moment was computed, as described previously (Eq. 33), for different occupancy levels. The results were fit to the theoretical model (Eq. 34) assuming four possible cases:

Model (I). The intracrystalline diffusivity, D_z, is concentration-dependent. The relationship between D_z and θ (the mean occupancy for each adsorption, or desorption, step) is obtained from the Darken equation:

$$D_z(\theta) = D_{z0}\left.\frac{d\ln(p)}{d\ln(q)}\right|_{\theta}. \quad (42)$$

This equation has been widely used to describe the concentration dependence of the diffusivity measured in different zeolite systems (Ruthven and Loughlin, 1971a,b; Ruthven et al., 1973; Vavlitis et al., 1981). D_{z0} is commonly designated as the "corrected diffusivity" (generally identified with the self-diffusivity) and its weak concentration-dependence may be neglected in this kind of measurement (Ruthven, 1984).

The derivative in Eq. 42 is obtained from the adsorption isotherm. Thus, from Eq. 40 we have:

$$D_z = D_{z0}\left(\frac{1}{1-\theta} + \beta\theta\right). \quad (43)$$

In addition, gas–phase mass-transfer resistance is assumed, and consequently $K(\theta)$ must be evaluated from Eq. 41.

After substitution, Eq. 34 becomes

$$M_1 = (\tau_{c1}+\tau_{c2}) + \frac{1}{15}\frac{R^2}{D_{z0}}\frac{1}{\frac{1}{1-\theta}+\beta\theta} + \frac{1}{3}\frac{R}{k_f}K(\theta). \quad (44)$$

The fitting parameters in the model are D_{z0} and k_f. $(\tau_{c1}+\tau_{c2})$ is estimated by direct extrapolation from the experimental data for $\theta \to 1$.

Model (II). D_z is again concentration-dependent, but now the more simple relationship is assumed:

$$D_z = D_{z0}\frac{1}{1-\theta}. \quad (45)$$

This result can be obtained from Eq. 42 in the case of an ideal Langmuir isotherm ($\beta = 0$). Even though the isotherms described in this work are not ideal, it is important to test the relationship of Eq. 45, since this is actually the form of the dependence commonly described in the literature.

In relation to the external mass-transfer resistance, the assumptions are the same as in model (I). The final expression for M_1 is then

$$M_1 = (\tau_{c1} + \tau_{c2}) + \frac{1}{15}\frac{R^2}{D_{z0}}(1-\theta) + \frac{1}{3}\frac{R}{k_f}K(\theta). \quad (46)$$

Once again, the fitting parameters are D_{z0} and k_f. $(\tau_{c1} + \tau_{c2})$ is estimated by direct extrapolation from the experimental data for $\theta \to 1$.

Model (III). D_z is not concentration-dependent. The variation of M_1 with occupancy is given only by the external gas–film resistance term:

$$M_1 = C + \frac{1}{3}\frac{R}{k_f}K(\theta), \quad (47)$$

where

$$C = (\tau_{c1} + \tau_{c2}) + \frac{1}{15}\frac{R^2}{D_z}.$$

C and k_f are the fitting parameters.

Model (IV). D_z is concentration-dependent, according to Eq. 43. The external resistance is now assumed to be at the particle surface, and is represented by k_s (invariant with loading). The corresponding term is therefore independent of θ:

$$M_1 = C + \frac{1}{15}\frac{R^2}{D_{z0}}\frac{1}{\dfrac{1}{1-\theta} + \beta\theta}, \quad (48)$$

where

$$C = (\tau_{c1} + \tau_{c2}) + \frac{1}{3}\frac{R}{k_s}.$$

C and D_{z0} are the parameters to estimate. Note that k_s is, so far, assumed as concentration-independent. The validity of this hypothesis will be discussed later.

Model (V). D_z is concentration-dependent, according to Eq. 43. The external resistance is associated to nonequilibrium sorption conditions at the surface. Micke and coworkers (Micke et al., 1994) used Langmuir kinetics to model this phenomenon. Their model leads to a pseudo surface barrier at the particle surface, with k_s being concentration-dependent:

$$k_s = k_a p + k_d = k_a \frac{\theta e^{\beta\theta}}{\alpha(1-\theta)} + k_d. \quad (49)$$

Then M_1 is given by

$$M_1 = (\tau_{c1} + \tau_{c2}) + \frac{1}{15}\frac{R^2}{D_{z0}}\frac{1}{\dfrac{1}{1-\theta} + \beta\theta} + \frac{1}{3}\frac{R}{k_a\dfrac{\theta e^{\beta\theta}}{\alpha(1-\theta)} + k_d}. \quad (50)$$

The fitting parameters are D_{z0}, k_a, and k_d.

One critical assumption is present in all these formulations. As discussed earlier, intracrystalline mass transport should be controlled by the erionite regions. Thus, the concentration dependence of D_z should be established in terms of the occupancy in these regions. However, only the total occupancy θ is known. We have, therefore, to assume uniform coverage of the entire framework for each step. The consequences of this assumption will be discussed later.

Experimental values of M_1 as a function of $(1-\theta)$ are plotted in Figures 7 to 9 for adsorption and desorption steps of heptane at 200, 250 and 300°C. The "best fits" of the models previously described are also shown [model (IV) is shown only in Figure 8]. A least-squares criterion was employed for these evaluations. We first note that the moments computed from adsorption and desorption steps are in good agreement. This was also confirmed by comparing the shape of the adsorption and desorption curves. Since we expect the moments computed from desorption steps to be closer to the "true" value, only these were used for the parameter estimation.

It was assumed that $(\tau_{c1} + \tau_{c2}) = 10$ s. This value was obtained from rough extrapolation of the data points at all temperatures for $\theta \to 1$ (the point at which the time constants for the other processes should vanish). The contribution of the nonideal gas–phase concentration step to the dynamics of the

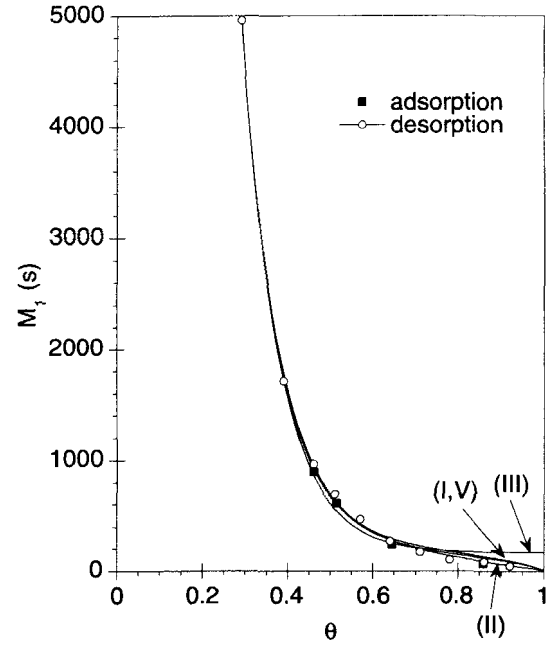

Figure 7. First moment data computed from heptane adsorption and desorption at 200°C.

The roman numeral on each line designates the model.

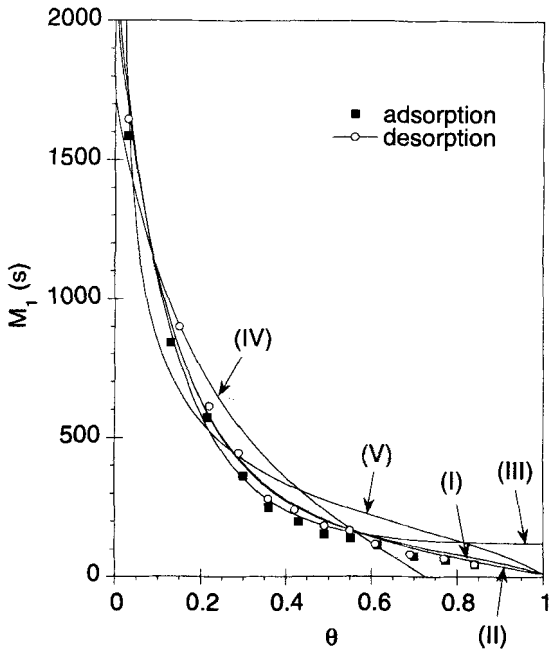

Figure 8. First moment data computed from heptane adsorption and desorption at 250°C.

The roman numeral on each line designates the model.

global transport process can then be assumed insignificant. This was also verified by observing that no significant change in the uptake curves occurred when the measurements were performed at different carrier gas-flow rates.

It is immediately clear that only models (I) and (II) fit the data properly over the entire range of occupancies and temperatures. Model (V) fits the data only at the lower temperature (200°C). The values of the parameters D_{z0} and k_f corresponding to the fits of models (I) and (II) are shown in Table 2.

Table 2. Parameters D_{z0} and k_f Obtained from Fitting Models (I) and (II) to Experimental Values of M_1 for Heptane

Temp. °C	Model (I) D_{z0} cm²/s	Model (I) k_f cm/s	Model (II) D_{z0} cm²/s	Model (II) k_f cm/s
200	1.41×10^{-13}	4.41×10^{-4}	3.82×10^{-13}	4.40×10^{-4}
250	4.41×10^{-13}	1.09×10^{-3}	7.54×10^{-13}	9.46×10^{-4}
300	1.71×10^{-12}	1.30×10^{-3}	2.75×10^{-12}	1.12×10^{-3}

The values obtained for D_{z0} and k_f were then used in Eq. 35 to compute the second moment. The results were then compared to the experimental values of M_2 (see Figures 10 and 11). The agreement is quite good, considering the expected larger error in the computation of M_2 from experimental data. Once again, only models (I) and (II) seem to describe the trend of the experimental data for all θ. Model (II) actually seems to give the best fits. Model (III) does not even reproduce the trend of the experimental data. Model (V) does not give satisfactory results at the two higher temperatures.

We can now attempt to estimate the activation energies corresponding to the intracrystalline and external resistance coefficients, even though we are aware of the limited precision involved in a computation based on only three temperatures. The corresponding Arrhenius plots are shown in Figures 12 and 13. Gorring's plot for n-heptane is also shown in Figure 12. His diffusivities are about one order of magnitude lower than the values reported here. The activation energies

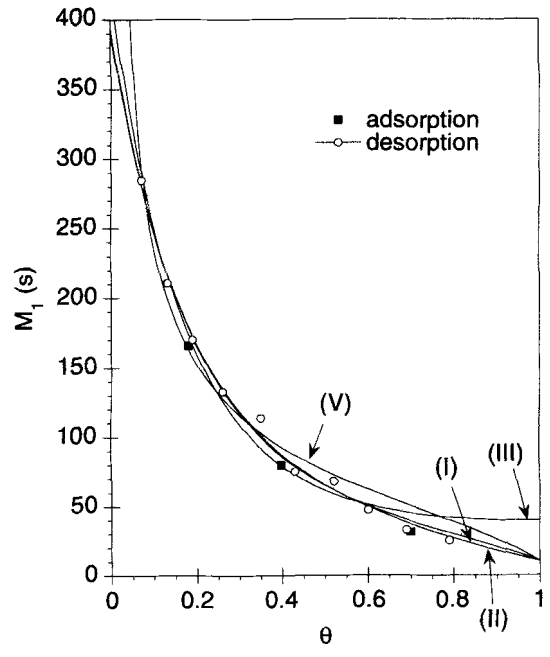

Figure 9. First moment data computed from heptane adsorption and desorption at 300°C.

The roman numeral on each line designates the model.

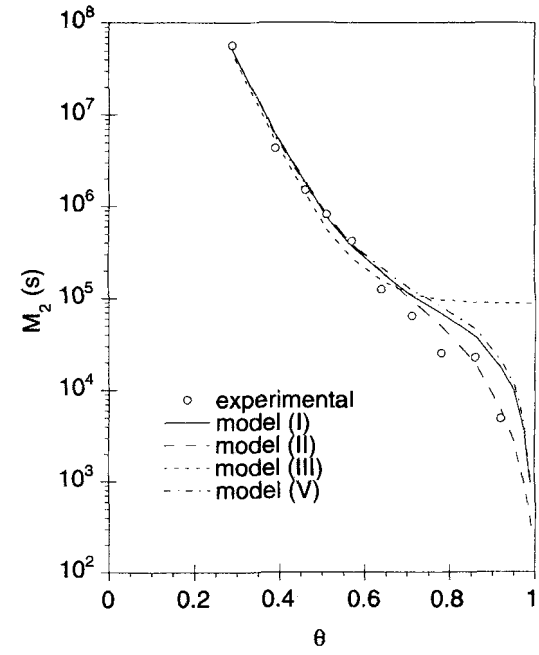

Figure 10. Second moment data computed from heptane desorption at 200°C.

The values from the models were computed using the parameters determined from the fittings of the first moment.

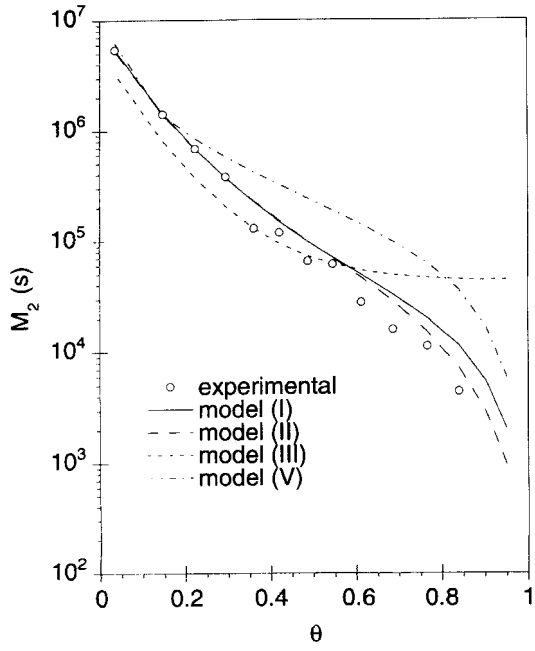

Figure 11. Second moment data computed from heptane desorption at 250°C.

The values from the models were computed using the parameters determined from the fittings of the first moment.

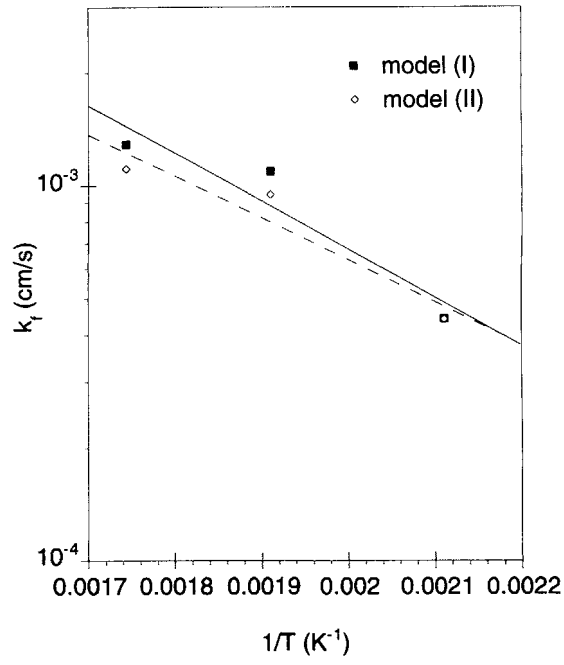

Figure 13. Arrhenius plots for external mass-transfer resistance coefficients of *n*-heptane obtained from models (I) and (II).

obtained from the estimates of models (I) and (II) (see Table 3) are 11% and 30%, respectively, lower than Gorring's.

Analysis of the individual contributions of the intracrystalline diffusion and external gas–film resistance terms to the first moment is shown in Figure 14, for model (I) [similar

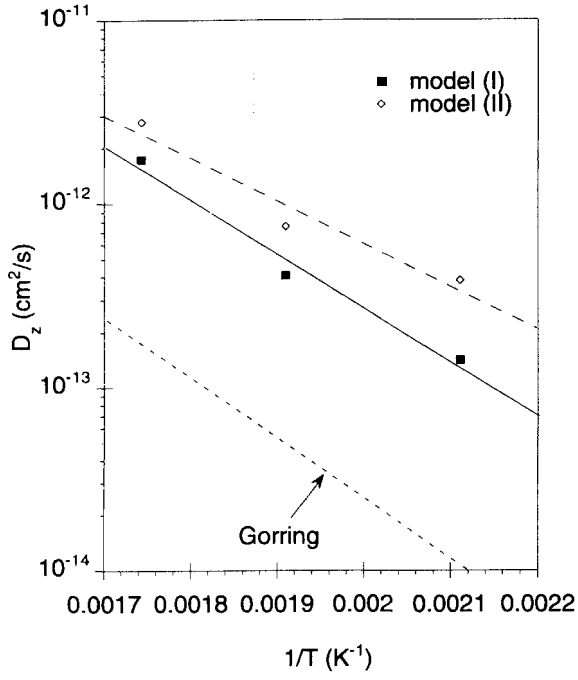

Figure 12. Arrhenius plots for diffusion coefficients of *n*-heptane obtained from models (I) and (II).

Gorring's result is also shown.

results can be obtained for model (II)]. At low occupancies, both terms are large, but the external resistance is the most important. As occupany increases, both terms decrease. The external resistance term, however, decreases more sharply, due to the strong dependence of $K(\theta)$ on concentration. The diffusion term does not decrease as rapidly, and becomes the major contribution to M_1 at high θ. An alternative way to perform this analysis is by computing Bi_m as a function of occupancy (Eq. 26) using the assumptions and estimated parameters of model (I). An example is shown in Figure 15. At low occupancies, Bi_m is quite low, reflecting the importance of the external resistance's contribution. As θ increases, Bi_m increases rapidly, and the intracrystalline diffusion becomes the controlling process.

In order to see how well the model can reproduce the uptake curves in the entire range of occupancies, values of τ_{diff} and Bi_m computed from the moments were used as initial guesses in the Fourier domain fitting of the uptake curves. A few examples of the resulting optimized curves are shown in Figure 16 as f vs. $\sqrt{t}$, and in Figure 17 as $\log(1-f)$ vs. t. As discussed earlier in this work, the optimized values of the parameters cannot be trusted as "best" solutions, since the

Table 3. Activation Energies, E_a, and Preexponential Factors, A, for D_z and k_f Computed from Models (I) and (II) and from Gorring's Results (Gorring, 1973)

	D_{z0}		k_f	
	E_a kJ/mol	A cm^2/s	E_a kJ/mol	A cm/s
Model (I)	56.3	2.03×10^{-7}	24.7	2.56×10^{-1}
Model (II)	44.3	2.58×10^{-8}	21.3	1.07×10^{-1}
Gorring	63.6	1.20×10^{-7}		

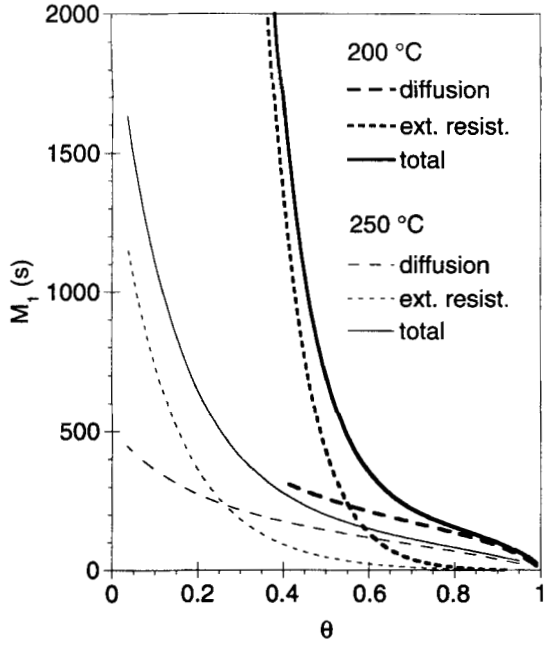

Figure 14. Contributions of the diffusion and external resistance terms to the first moment computed by model (I).

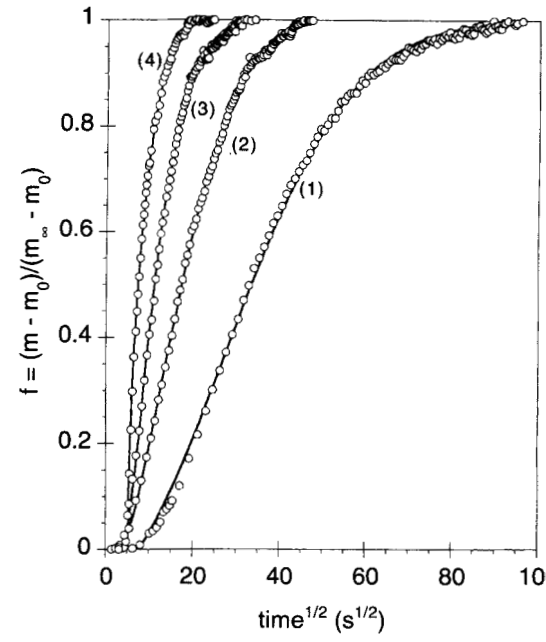

Figure 16. Experimental desorption curves for heptane at 250°C, compared to theoretical curves obtained from Fourier domain fitting.

The numbers on the curves designate the following optimized parameters: (1) $\theta = 0.04$, $\tau_{diff} = 9.21 \times 10^3$, $Bi_m = 1.22$; (2) $\theta = 0.29$, $\tau_{diff} = 2.28 \times 10^3$, $Bi_m = 2.76$; (3) $\theta = 0.49$, $\tau_{diff} = 1.88 \times 10^3$, $Bi_m = 18.9$; (4) $\theta = 0.69$, $\tau_{diff} = 7.53 \times 10^2$, $Bi_m = 54.7$.

fitting procedure is strongly affected by local minima. The only purpose of the results shown is to prove that the model can reproduce the experimental uptake data. Note that the optimized parameters follow the same trend as previously discussed: low Bi_m at low θ, much higher Bi_m at higher occupancies.

So far in the present discussion, we have found that the experimental results are well described only by the models involving the gas–phase resistance formulation (models (I) or (II)). However, an inconsistency can be seen in the computed values of k_f, the gas–film mass-transfer coefficient. Indeed, from Table 2, k_f is around 10^{-3} cm/s. This value is very low

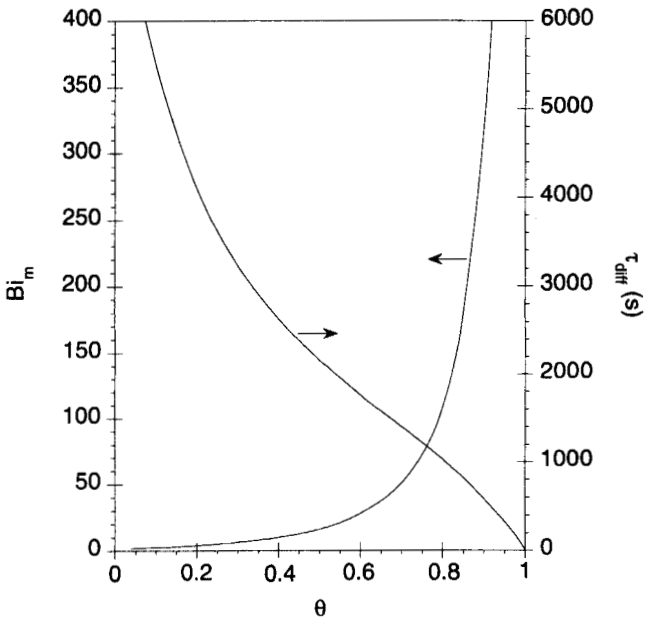

Figure 15. Values of Bi_m and τ_{diff} corresponding to the fit of model (I) to heptane desorption at 250°C.

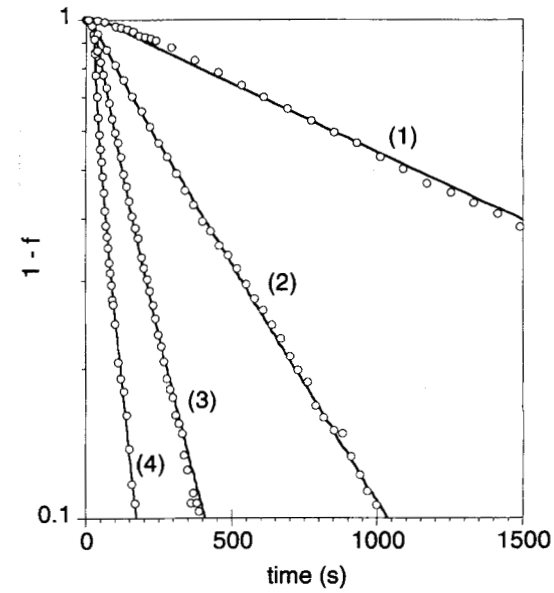

Figure 17. Experimental desorption curves for heptane at 250°C, compared to theoretical curves obtained from Fourier domain fitting.

The numbers on the curves designate the same parameters as in Figure 16.

for this type of resistance. Molecular diffusion of n-heptane in helium is about 0.92 cm^2/s (estimated from Reid et al., 1987). Considering a stagnant film of gas around the zeolite particle ($Sh = 2$), one would have

$$k_f = \frac{Sh\, D_m}{2R} = 3.2 \times 10^4 \text{ cm/s}. \tag{51}$$

If one assumes Knudsen diffusion in the intercrystalline space, then the gas-phase diffusivity would be $D_k \sim 10^{-4}$ cm^2/s (for an intercrystalline pore radius of 1 μm). Using the same relationship as in Eq. 51, k_f would now be in the order of 1 cm/s, which is still too large. These results lead us to consider that the transport resistance is associated with a framework-related surface barrier (constrictions of the pore entrances). However, we have seen that model (IV) fails completely in describing the measured data (see Figure 8). We believe that analysis of the values of k_f indicates that we are dealing with a resistance mechanism that is more complex than initially presumed. However, the mathematical formulation of the model is still valid. Further verification of its consistency will be given below.

It may be interesting to analyze in more detail the association of the local slope of the isotherm to a gas-phase resistance model, since this is the essential difference between the formulations of the gas-phase and particle-surface resistance models. This can be better understood with the help of a simple schematic representation of the concentration profiles involved (Figure 18). Consider a gas-phase resistance (Figure 18a). Initially, the concentration in the bulk gas is C_{b0} and inside the particle is q_0. During an adsorption step so that the final intraparticle concentration becomes q_∞, then the outside gas concentration must be increased to $C_{b\infty}$. Assuming local linearity of the isotherm:

$$(C_{b\infty} - C_{b0}) = \frac{1}{K}(q_\infty - q_0). \tag{52}$$

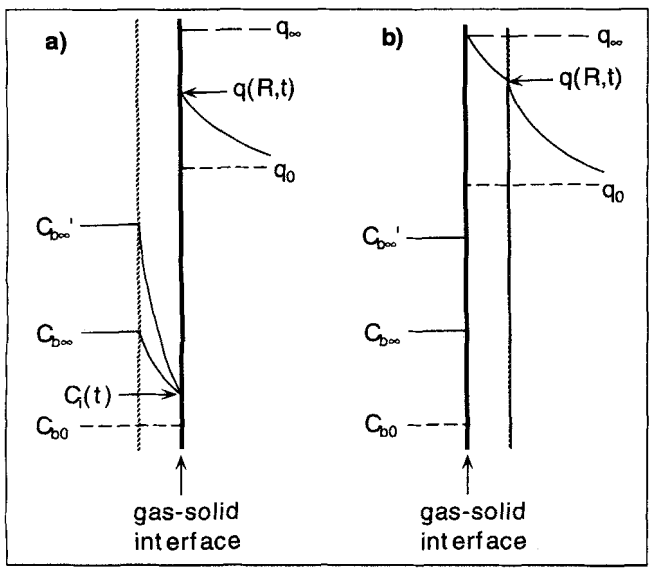

Figure 18. Concentration profiles when extra-crystalline mass-transfer resistance is located at (a) external gas-phase, (b) particle surface.

During this adsorption step, the concentration in the gas phase at the interface will be $C_i(t)$, in equilibrium with $q(R,t)$, the concentration at the particle surface. The driving force for mass transfer across the gas film is proportional to $[C_{b\infty} - C_i(t)]$. For a similar adsorption step (final concentration inside the particle is q_∞), but with a lower value for the local slope of the isotherm ($K' < K$), the concentration in the bulk gas phase would have been obtained from

$$(C_{b\infty}' - C_{b0}) = \frac{1}{K'}(q_\infty - q_0) > (C_{b\infty} - C_{b0}). \tag{53}$$

In other words, the concentration step in the gas phase ($C_{b\infty}' - C_{b0}$) would have to be higher than before. As a consequence, the driving force across the gas film would also have been higher (see figure), implying faster mass transfer through the film. In the case of a particle surface resistance (Figure 18b), the driving force is located in the surface of the solid, and does not depend on $C_{b\infty}$ (and thus on K).

Some critical assumptions associated with the previous models also deserve some attention. Relationships between D_z and θ, the total occupancy in the particle, were described in Eqs. 43 and 45. However, as pointed out before, D_z should be related to the occupancy in the erionite regions only. It can be argued that, if this deviates significantly from θ, the suggested forms for $D_z(\theta)$ would not be valid; a corrected relationship might admit a better fit of model (IV) to the data. But whatever formulation is chosen for the variation of D_z with loading, a surface resistance model would still be intrinsically incompatible with the experimental results. Recall that such a model implies that $K(\theta)$ does not appear in the definition of Bi_m:

$$Bi_m = \frac{k_s R}{D_z}. \tag{27}$$

This way, the dependence of Bi_m on loading is given only by D_z (k_s is, so far, assumed independent of θ). Since M_1 decreases by several orders of magnitude with loading, the diffusivity also will have to increase by orders of magnitude. Consequently, Bi_m at low loadings must be significantly larger than at high loadings. This is incompatible with the observed shape of the uptake curves. In Figure 19 a few examples are shown for uptake at 200 and 250°C and different loadings. The slopes increase with occupancy because D_z increases. But the critical observation is that the curves corresponding to higher occupancies show some curvature. This is characteristic of diffusion-controlled transport (high Bi_m). At lower occupancies, on the other hand, the curves are essentially linear, clearly indicating stronger extracrystalline resistance (lower Bi_m). These observations are totally compatible with the previous analysis of models (I) and (II). Indeed, for a gas-phase resistance,

$$Bi_m = \frac{k_f R}{D_z K}. \tag{26}$$

The increase of D_z is overcome by the stronger dependence of K on occupancy. As a result, Bi_m increases with θ. This shows that the consistency of the gas-phase resistance model

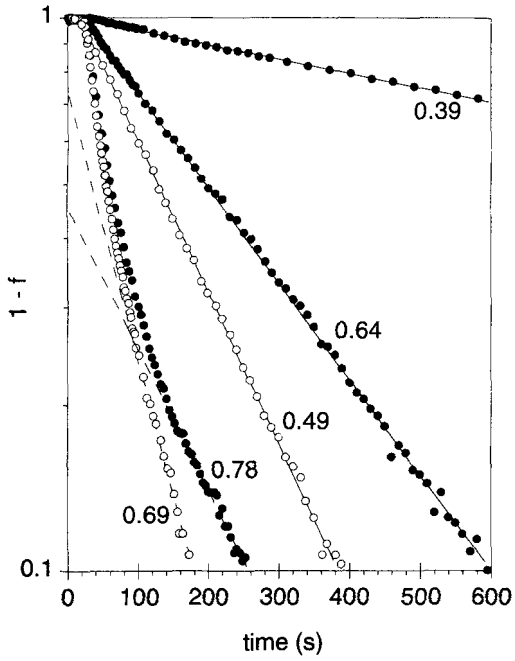

Figure 19. Uptake curves for *n*-heptane desorption.

The numbers on the curves correspond to the mean occupancy of the desorption step, θ. Full circles: 200°C; empty circles: 250°C.

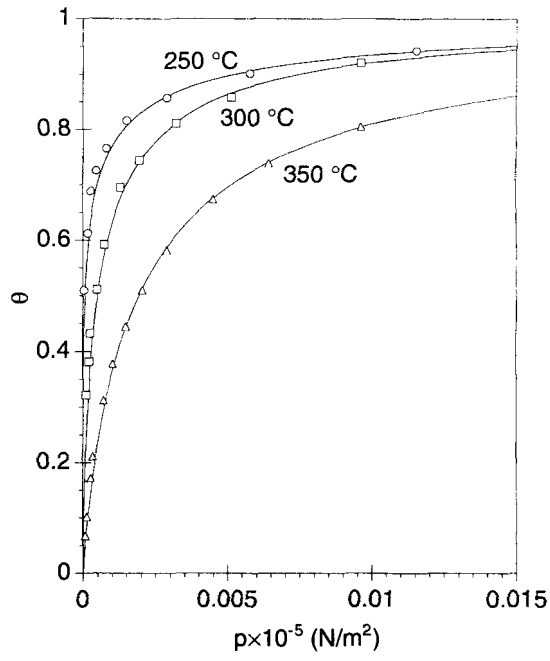

Figure 20. Isotherms for *n*-nonane sorption.

The curves correspond to the fits of Eq. 40 to the experimental data.

with the experimental results is not limited to the temporal moments data.

Note that a new element may be introduced in the discussion of the surface-resistance model if k_s were to depend on occupancy. Since the nature of the surface resistance is unknown, discussion of this aspect is very restricted. If the surface barrier is structural, then k_s may change with occupancy in a way similar to D_z. On the other hand, as shown in model (V), a loading-dependent k_s may result from nonequilibrium sorption at the surface. This model did not, however, fit the data as well as models (I) and (II).

Another test of the consistency of the results obtained with the gas–phase resistance model is to compare these to values of k_f computed from the slope of $\ln(1-f)$ vs. time plots, for the lower-occupancy curves. As pointed out in the Theory section, the values of k_f computed directly from the plots will coincide with the "true" coefficients only when the external resistance controls the mass-transfer process. If both external resistance and intracrystalline diffusion are important, the plots will still be linear, but the computed k_f will be lower than the true value (see Figure 3). Some results are shown in Table 4. Equation 28 was used to calculate k_f, with $K(\theta)$ computed from Eq. 41. Calculated values of k_s, from Eq. 29, are also shown in Table 4. As expected, the computed values of k_f are somewhat lower than the models' estimates (Table 2). The agreement is still quite good, though, in particular at lower occupancies (when the contribution from the external resistance is higher) and for model (II). The particularly good agreement obtained at 200°C would be expected, since it is at this temperature that the external resistance (at low loadings) more strongly dominates the diffusional term (see Figure 14).

It is interesting to note that Bülow and coworkers (Bülow et al., 1980) estimated values of k_s between 10^{-5} and 10^{-7} cm/s for sorption of *n*-hexane on MgA zeolite in the same temperature range, applying a model equivalent to Eq. 29 to low occupancy data.

Values of D_{z0} can also be estimated directly from the uptake data. As previously discussed, the higher occupancy curves reflect a diffusion-controlled transport. In these conditions, $D_z(\theta)$ can be estimated from the linear portion of the uptake curves (corresponding to long times), according to Eq. 32. Then D_{z0} can be obtained from Eqs. 43 or 45. Values estimated in this way agreed within 5 to 30% with the results from the first moment fittings. This again supports the validity of the model.

Table 4. Values of k_f and k_s Computed from Eqs. 28 and 29, Respectively*

Temp. °C	θ	k_f cm/s	k_f-k_f (I) %	k_f-k_f (II) %	k_s cm/s
200	0.29	4.41×10^{-4}	0	0.2	4.00×10^{-9}
	0.39	3.75×10^{-4}	15	15	1.12×10^{-8}
250	0.04	7.87×10^{-4}	28	17	1.18×10^{-8}
	0.15	6.18×10^{-4}	43	35	2.15×10^{-8}
300	0.07	8.91×10^{-4}	31	20	7.33×10^{-8}
	0.14	8.25×10^{-4}	36	26	1.00×10^{-7}

*The relative differences between these values of k_f and the estimates from models (I) and (II) are also shown.

Table 5. Parameters α and β Obtained from Fitting Eq. 40 to Experimental Sorption Data of *n*-Nonane

Temp. °C	α $(N/m^2)^{-1}$	β
250	1.83	5.19
300	4.00×10^{-2}	1.34
350	7.19×10^{-3}	0.651

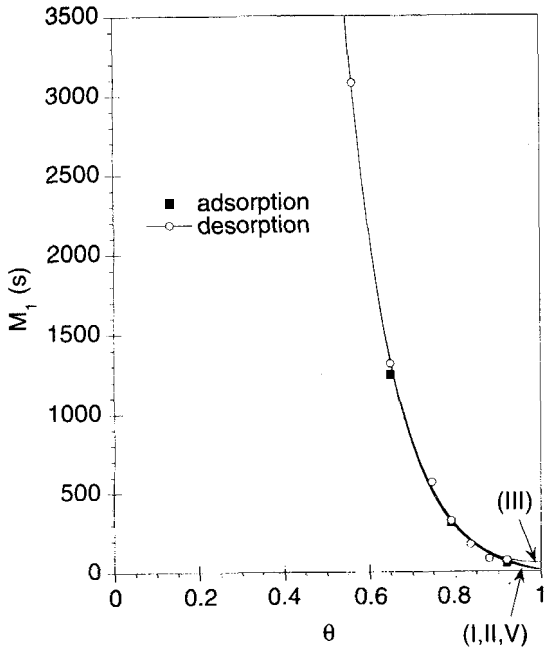

Figure 21. First moment data computed from nonane adsorption and desorption at 250°C.

The roman numeral on each line designates the model.

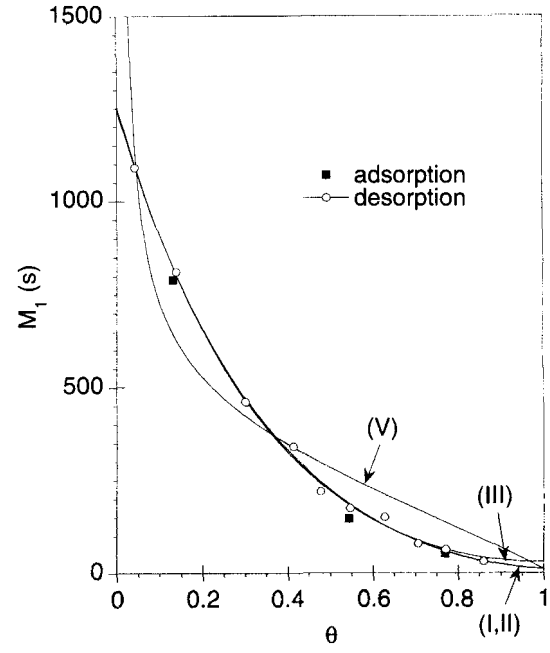

Figure 23. First moment data computed from nonane adsorption and desorption at 350°C.

The roman numeral on each line designates the model.

n-Nonane

Isotherms. The sorption isotherms obtained for *n*-nonane are shown in Figure 20. The computed parameters, from the fitting of Eq. 40, are shown in Table 5. These curves are steeper in the lower occupancy regions than the ones for *n*-heptane.

Transient mass transfer. The analysis of the mass-transfer dynamics for *n*-nonane was done in the same way as for *n*-heptane. Plots of the first moment of the uptake curves, as a function of occupancy, and the corresponding fits of the models are shown in Figures 21 to 23. Models (I) and (II) once again give the best fits. Model (V) is acceptable only at the lower temperature (250°C).

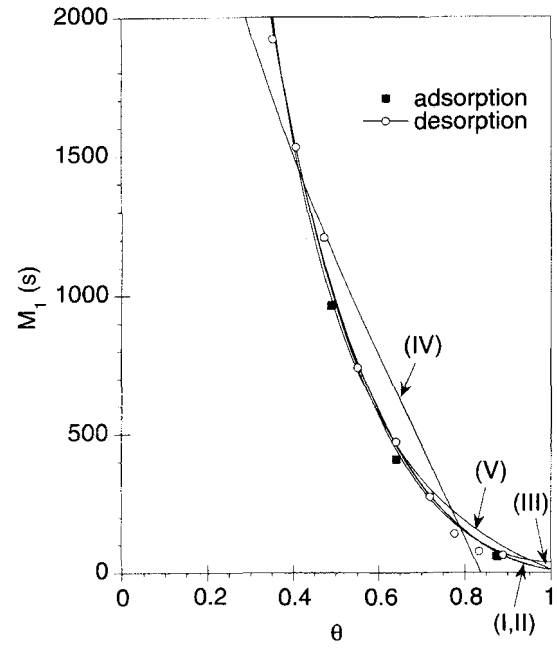

Figure 22. First moment data computed from nonane adsorption and desorption at 300°C.

The roman numeral on each line designates the model.

The computed values of D_{z0} and k_f obtained from models (I) and (II) are shown in Table 6. Once again, it was assumed $(\tau_{c1} + \tau_{c2}) = 10$ s. An example of the comparison between the values of the second moments computed from these parameters and the experimental results can be seen in Figure 24.

As a first observation, one notes that the plots of models (I) and (II) are now indistiguishable, with both describing well the measured data. This is due to the smaller (in relation to heptane's) relative contribution of the diffusional resistance term to the moments. Recall that the two models differ only in the form of this term. The ratio of the external and diffusional resistance terms in Eq. 44 for heptane and nonane at 250°C is shown in Figure 25. It is clear that the external resistance term largely overcomes the diffusional term at low occupancies.

It is striking that the first moments measured at low occupancies are much larger for nonane, at the same tempera-

Table 6. Parameters D_{z0} and k_f Obtained from Fitting Models (I) and (II) to Experimental Values of M_1 for *n*-Nonane

	Model (I)		Model (II)	
Temp °C	D_{z0} cm²/s	k_f cm/s	D_{z0} cm²/s	k_f cm/s
250	3.18×10^{-13}	1.52×10^{-4}	6.64×10^{-13}	1.53×10^{-4}
300	8.98×10^{-13}	2.27×10^{-4}	1.07×10^{-12}	2.29×10^{-4}
350	2.49×10^{-12}	3.22×10^{-4}	3.07×10^{-12}	3.18×10^{-4}

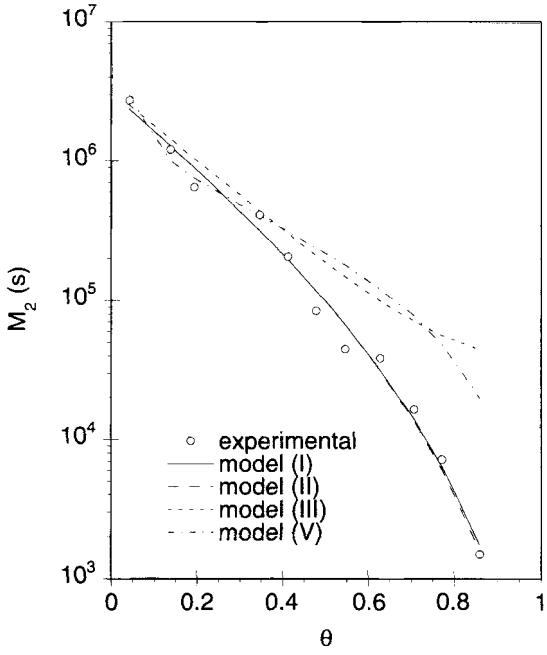

Figure 24. Second moment data computed from nonane desorption at 350°C.

The values from the models were computed using the parameters determined from the fittings of the first moment.

tures. According to models (I) and (II), this is a consequence of the larger external resistance term, due to the lower values of k_f (cf. Tables 2 and 6) and higher initial slopes of the isotherms. The diffusional term, even though it is also higher for nonane (cf. D_{z0} in Tables 2 and 4), does not contribute significantly for the first moment, as seen in Figure 25.

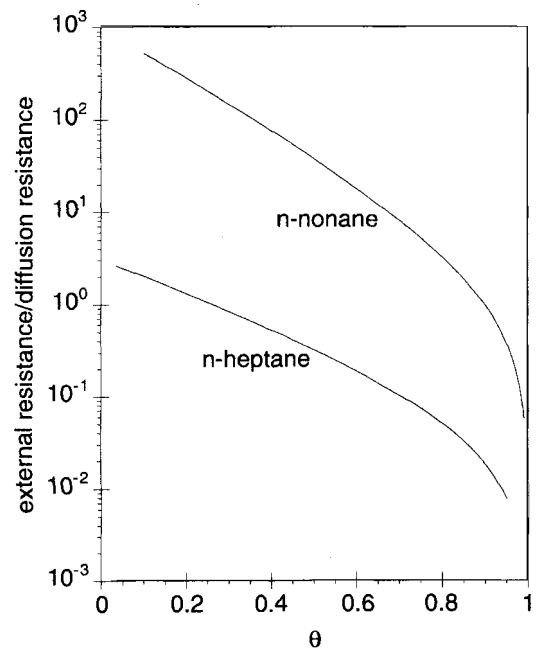

Figure 25. Ratio between the external resistance and diffusional resistance terms in the expression of the first moment—model (I).

Table 7. Values of k_f and k_s Computed from Eqs. 28 and 29, Respectively, for *n*-nonane*

Temp. °C	θ	k_f cm/s	$k_f - k_f$ (I) %	$k_f - k_f$ (II) %	k_s cm/s
250	0.56	1.41×10^{-4}	7	7	5.89×10^{-9}
	0.65	1.33×10^{-4}	12	12	1.34×10^{-8}
300	0.35	2.09×10^{-4}	8	9	9.33×10^{-9}
	0.41	1.88×10^{-4}	17	18	1.09×10^{-8}
350	0.041	3.00×10^{-4}	7	6	1.74×10^{-8}
	0.14	2.58×10^{-4}	20	19	2.06×10^{-8}

*The relative differences between these values of k_f and the estimates from models (I) and (II) are also shown.

The analysis of the shape of the uptake curves leads to the same results as for heptane: at high occupancies the log $(1-f)$ vs. t plots are concave upwards, characteristic of diffusion control, while at low occupancies the plots are linear, indicating that external resistance is dominant.

Values of k_s and k_f were also computed directly from the experimental $\ln(1-f)$ vs. t plots at lower occupancies, according to Eqs. 28 and 29. The results are shown in Table 7. The agreement between the values of k_f computed in this way and obtained from models (I) and (II) is very good. Notice that this is true even at the higher temperatures. For heptane, the discrepancy increased with temperature. One would expect this to happen, since for nonane the external resistance is largely dominant in the entire range of temperatures analyzed. For heptane, however, the two resistances were closer at higher temperatures, and there would be a larger error in estimating k_f directly from the uptake curves.

Also as with *n*-heptane, D_{z0} was estimated from the slopes of the long-time portion of the higher occupancy curves. The results were within 30% of the first moment fitting estimates.

The computed activation energies and preexponential factors are shown in Table 8. The corresponding Arrhenius plots are shown in Figures 26 and 27. The activation energies for both D_{z0} and k_f are practically identical for heptane and nonane. The preexponential factors show more significant differences, and are lower for nonane.

n-Dodecane

The low volatility of *n*-dodecane resulted in adsorbate condensate in the sample hanging wire and in some internal glass walls, at high gas-phase concentrations. Consequently, adequate control of the gas-phase concentration steps and measurements at high occupancies were not possible. Therefore, reliable data for the statistical moments analysis could not be obtained with this adsorbate. However, since parameter esti-

Table 8. Activation Energies, E_a, and Preexponential Factors, A, for D_z and k_f Computed from Models (I) and (II) and from Gorring's Results (Gorring, 1973) for *n*-Nonane

	D_{z0}		k_f	
	E_a kJ/mol	A cm²/s	E_a kJ/mol	A cm²/s
Model (I)	55.8	1.13×10^{-7}	19.9	1.48×10^{-2}
Model (II)	41.0	7.36×10^{-9}	19.9	1.47×10^{-2}
Gorring	62.0	8.50×10^{-8}		

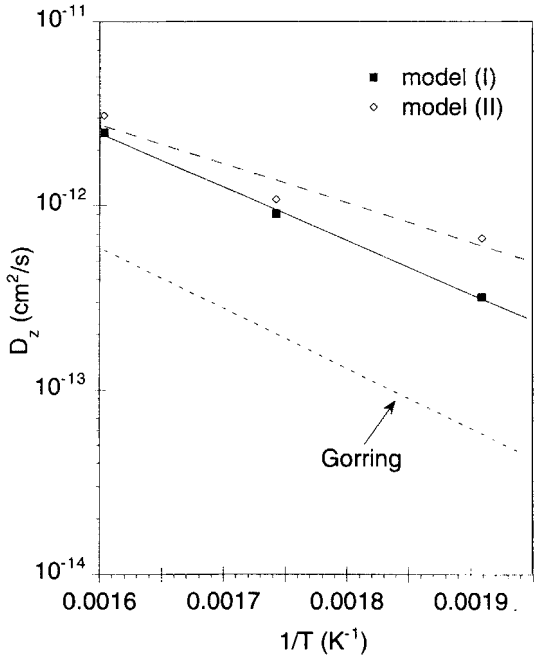

Figure 26. Arrhenius plots for diffusion coefficients of *n*-nonane obtained from models (I) and (II).

Gorring's result is also shown.

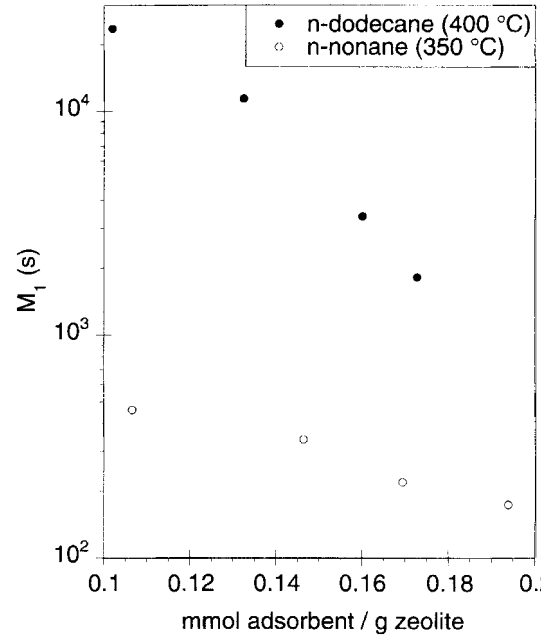

Figure 28. First moment data obtained for *n*-dodecane at 400°C.

Data for *n*-nonane at 350°C is also shown for comparison.

mation directly from the uptake curves had proved reasonably accurate in the two previous cases, we used this approach in order to obtain estimates for D_{z0} and k_f. We were able to measure uptake curves at high enough concentration to obtain the characteristic curvature indicative of diffusion control. From these, a diffusivity of $D_{z0} \sim 1 \times 10^{-13}$ cm²/s at 300°C was estimated. From the low occupancy curves a value of $k_f \sim 4 \times 10^{-5}$ cm/s was calculated, at the same temperature.

Some first moment data at low occupancy is shown in Figure 28. It is striking how much longer the time constant is for transport of *n*-dodecane. This is a consequence of the lower k_f and the steeper isotherm [and, thus, larger $K(\theta)$].

It is essential to recall that the original objective of the present work is the study of the existence of the window effect. The major feature of the Gorring data consisted in the 100-fold increase of diffusivity relative *n*-heptane or *n*-nonane. Our estimates indicate that D_{z0} for *n*-dodecane is definitely not higher than for the other two species. Indeed, we have calculated diffusion coefficients at 300°C of 1.71×10^{-12}–2.75×10^{-12} cm²/s (depending on whether Eq. 43 or 45 was used) for *n*-heptane, and of 8.98×10^{-13}–1.07×10^{-12} cm²/s for *n*-nonane. On the other hand, the diffusivity estimated for *n*-dodecane was 1×10^{-13} cm²/s.

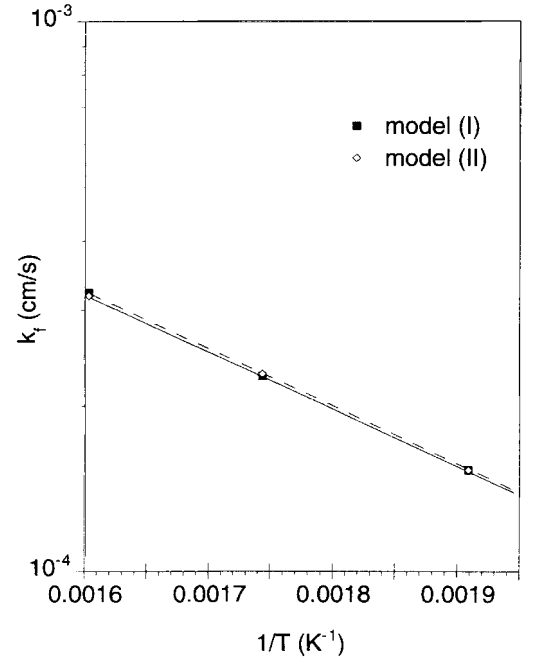

Figure 27. Arrhenius plots for external resistance coefficients of *n*-nonane obtained from models (I) and (II).

Conclusions

Nondiffusional transport significantly affects the mass transfer of *n*-paraffins in the sample of zeolite T studied. It was shown that a model involving intracrystalline diffusion (occupancy-dependent) and external (nondiffusional) mass-transfer resistance (dependent on the local slope of the sorption isotherm) describes well the first and second moment data. The transport parameters estimated from the first moment data are consistent with the observed shape of the uptake curves and with the values estimated directly from the curves. At low loadings, mass transfer is strongly limited by the external resistance. Closer to saturation, however, the process becomes controlled by intracrystalline diffusion.

The low magnitude of the values computed for the external resistance mass-transfer coefficient, k_f, and its relatively high activation energy, indicate that this process may be associated with transport within the solid phase, that is, at the particle surface. The theories of thermal, evaporation, or conformational barriers are not compatible with the good agreement observed between the adsorption and desorption data. The hypothesis of a "surface barrier" being due to framework modifications at the crystal surface, as reported in the literature for hydrothermally pretreated samples of zeolite A (Bülow et al., 1982), does not, by itself, justify the verified importance of the local slope of the isotherm in the description of the experimental results. Entropic effects involved in the adsorption/desorption at the surface may be important. The nonequilibrium sorption model did not fit satisfactorily all the data. It did, however, show the same qualitative trends as our results, and also involves a loading-depending external resistance term.

No evidence of the existence of a window effect was found. The estimated diffusional parameters, D_{z0}, decrease continuously with chain length, contrary to Gorring's results. The activation energy for diffusion, however, is similar for *n*-heptane and *n*-nonane (about 48 kJ/mol). This agrees with Ruthven's observations for *n*-paraffin diffusion in zeolites 5A, silicalite and NaX (Ruthven and Eic, 1988; Vavlitis et al., 1981): after initially increasing with chain length, activation energies become essentially constant above a certain carbon number; on the other hand, the preexponential factors decrease continuously. Barrer (1983), based on similar results obtained by Kärger with NMR experiments in NaX (Kärger et al., 1980), suggested that this behavior is due to segmental diffusion of the chain. This effect is attributed to the segmental rotation of part of a linear molecule about a C-C bound, resulting in changes in the center of mass of the molecule without necessarily involving simultaneous translation of all parts of the chain. If the mechanism involves segments of approximately constant size above a certain chain length, then the activation energy becomes almost constant. Also, since for a longer chain more diffusion unit steps are necessary for migration of the entire molecule between sites, the preexponential factor must decrease with chain length. The magnitudes of the estimated values of the diffusional activation energy and diffusion coefficients are characteristic of a small-pore zeolite (cf. Kärger and Ruthven, 1992c), which supports the assumption that intracrystalline transport is limited by the erionite phase.

In relation to the nondiffusional resistance parameter, k_f, the activation energy is again similar for *n*-heptane and *n*-nonane (about 22 kJ/mol). The fact that, despite this, k_f decreases significantly with chain length (note that its preexponential factor is an order of magnitude lower for nonane than for *n*-heptane), may indicate that chain-length-dependent entropic effects are involved in the transport through the external barrier.

Since Gorring did not show plots of the uptake curves, we cannot analyze the possibility of nondiffusional effects (sigmoidal curves) in his data. Also, Gorring states that the diffusion coefficient does not vary significantly with concentration up to 80% of the saturation loading. Above 80% saturation diffusivities were said to decline. This is in strong disagreement with our results, since we observed a very pronounced decrease of the transport time constants (an increase in diffusivity) with occupancy. It is not possible to conclude whether these discrepancies are due to differences in the nature or treatment of the samples, or to deficiencies in Gorring's experimental procedure. Aspects such as heat dissipation, mass-transfer resistance in the sample bed (Gorring reports using 5.38 g of sample!), sorbate condensation in components of the balance, or sample modifications (such as coking) throughout the studies (it is reported that the same sample was used in all experiments) may have affected his results.

The approach developed in this work for isolating intracrystalline and external mass-transfer resistances provides a good description of the experimental data, and leads to consistent results. The method is based on the analysis of the occupancy dependence of the temporal moments of the transient uptake curves and a simple mass-transfer model.

Even though some ambiguity remains regarding the nature of the nondiffusional resistance, we believe that this work introduces valuable new elements into the study of mass transport in zeolites.

Notation

A = preexponential factor in Arrhenius equation, cm^2/s
$C_{b,eq}$ = equilibrium bulk gas-phase adsorbate concentration, mol/cm^3
$\overline{C}_i$ = gas-phase adsorbate concentration at the gas-solid interface (shift variable), mol/cm^3
D_{eri} = diffusion coefficient in the erionite phase, cm^2/s
D_{off} = diffusion coefficient in the offretite phase, cm^2/s
E_a = activation energy, kJ/mol
$\hat{g}(m)$ = Fourier transform of $g(t)$
k_a = Langmuir kinetic constant for adsorption at the crystal surface, cm/bar·s
k_d = Langmuir kinetic constant for desorption at the crystal surface, cm/s
k_f = mass-transfer coefficient associated with a gas-film resistance model, cm/s
L = Laplace transform operator
m_0 = mass adsorbed at the beginning of adsorption (desorption) step, g
m_{max} = mass of adsorbate adsorbed at saturation conditions, g
m_{sample} = mass of zeolite sample, g
m_∞ = mass adsorbed at the end of adsorption (desorption) step, g
M_w = adsorbate molecular weight
p = adsorbate pressure in the gas phase, N/m^2
q_{eq} = equilibrium solid-phase adsorbate concentration, mol/cm^3
r = radial coordinate, cm
R = particle radius, cm
R_g = ideal gas constant
s = Laplace transform parameter, s^{-1}
Sh = Sherwood number
T = temperature, K
ϕ_{off} = offretite phase volume fraction
τ_{c1}, τ_{c2} = time constants associated to the nonideal bulk gas-phase concentration step, s

Literature Cited

Abramowitz, M., and I. A. Stegun, *Handbook of Mathematical Functions*, Dover, New York (1965).

Arnould, D., and R. L. Laurence, "Solute Diffusion in Polymers by Capillary Column Inverse Gas Chromatography," *Inverse Gas Chromatography*, D. R. Lloyd, H. P. Schreiber, and T. C. Ward, eds., Amer. Chem. Soc., Washington, DC, p. 87 (1989).

Barrer, R. M., "Intracrystalline Diffusion," *Adv. in Chem.*, **102**, 1 (1971).

Barrer, R. M., "Sorption by Zeolites: II. Kinetics and Diffusivities," *Zeolites: Science and Technology. NATO ASI Ser.*, Alcabideche, Portugal, p. 261 (1983).
Barrer, R. M., "Flow Into and Through Zeolite Beds and Compacts," *Langmuir*, **3**, 309 (1987).
Barrer, R. M., and D. L. Peterson, "Kinetics of *n*-Paraffin Sorption in the Natural Zeolite Erionite," *J. Phys. Chem.*, **68**, 3427 (1964).
Bennett, J. M., and J. A. Gard, "Non-Identity of the Zeolites Erionite and Offretite," *Nature*, **214**, 1005 (1967).
Breck, D. W., *Zeolite Molecular Sieves*, Wiley, New York, p. 507 (1974a).
Breck, D. W., *Zeolite Molecular Sieves*, Wiley, New York, p. 48 (1974b).
Bülow, M., "Molecular Mobility of Single Components and Mixtures on Zeolites," *Chemistry of Microporous Crystals; Proceedings of the International Symposium on Chemistry of Microporous Crystals*, Elsevier, Tokyo, p. 199 (1991).
Bülow, M., and P. Struve, "Experimental Evidence of the Influence of Sorption-Heat Release Processes on the Sorption Kinetics of Benzene in NaX Zeolite Crystals," *J. Chem. Soc., Faraday Trans. I*, **80**, 813 (1984).
Bülow, M., P. Struve, G. Finger, C. Redszus, K. Ehrhardt, and W. Schirmer, "Sorption Kinetics of *n*-Hexane on MgA Zeolites of Different Crystal Sizes," *J. Chem. Soc. Farad. Trans. I*, **76**, 597 (1980).
Bülow, M., P. Struve, and S. Pikus, "Influence of Hydrothermal Pretreatment on Zeolitic Diffusivity Detected by Comparative Sorption Kinetics and Small-Angle X-Ray Scattering Investigations," *Zeolites*, **2**, 267 (1982).
Bülow, M., P. Struve, C. Redszus, and W. Schirmer, "Sorption Kinetics of n-Decane on MgA Type Zeolites of Different Crystal Size," *Proc. Int. Conf. on Zeolites*, Naples, p. 580 (1980).
Bülow, M., P. Struve, and L. V. C. Rees, "Investigation of the Gaseous Phase Diffusion and Liquid Phase Self-Diffusion of *n*-Decane on NaCa-A Zeolites," *Zeolites*, **5**, 113 (1985).
Chen, N. Y., "Offretite-T-Erionite Catalytic Characterization," *Proc. Int. Cong. on Catal.*, Miami Beach, FL, p. 1343 (1972).
Chen, N. Y., S. J. Lucki, and E. B. Mower, "Cage Effect on Product Distribution from Cracking over Crystalline Aluminosilicalite Zeolites," *J. Catal.*, **13**, 329 (1969).
Crank, J., *The Mathematics of Diffusion*, Chap. 6, Clarendon Press, Oxford (1975).
Dubinin, M. M., I. T. Erashko, O. Kadlec, and V. I. Ulin, "Kinetics of Physical Adsorption by Carbonaceous Adsorbents of Biporous Structure," *Carbon*, **13**, 193 (1975).
Froment, G. F., and K. B. Bischoff, *Chemical Reactor Analysis and Design*, Wiley, New York (1990).
Garg, D. R., and D. M. Ruthven, "The Effect of the Concentration Dependence of Diffusivity on Zeolitic Sorption Curves," *Chem. Eng. Sci.*, **27**, 417 (1972).
Gorring, R. L., "Diffusion of Normal Paraffins in Zeolite T," *J. Catal.*, **31**, 13 (1973).
Kärger J., "A Study of Fast Tracer Desorption in Molecular Sieve Crystals," *AIChE J.*, **28**, 417 (1982).
Kärger, J., M. Bülow, V. I. Ulin, A. M. Voloshchek, P. P. Zolotarev, M. Kocirik, and A. Zikánová, "On the Importance of Dimension Variation in Determining the Limiting Steps in Adsorption Kinetics," *J. Chem. Tech. Biotechnol.*, **32**, 376 (1982).
Kärger, J., H. Pfeifer, M. Rauscher, and M. Bülow, "Comparative NMR and Uptake Studies of Molecular Transport of Ethane in 5A Zeolites after Different Sample Pretreatment," *Z. Phys. Chem.*, **262**, 567 (1981).
Kärger, J., H. Pfeifer, M. Rauscher, and A. Walter, "Self-Diffusion of n-Paraffins in NaX Zeolite," *J. Chem. Soc. Trans. Farad. I.*, **76**, 717 (1980).
Kärger, J., H. Pfeifer, R. Richter, and H. Fürtig, "NMR Study of Mass Transfer in Granulated Molecular Sieves," *AIChE J.*, **34**, 1185 (1988).
Kärger, J., H. Pfeifer, R. Seidel, and B. Staudte, "Investigation of Surface Barriers on CaNaA Type Zeolites by Combined Application of the N.M.R. Tracer Desorption Method and X-Ray Photoelectron Spectroscopy," *Zeolites*, **7**, 282 (1987).
Kärger, J., and D. M. Ruthven, "On the Comparison between Macroscopic and N.M.R. Measurements of Intracrystalline Diffusion in Zeolites," *Zeolites*, **9**, 267 (1989).
Kärger, J., and D. Ruthven, *Diffusion in Zeolites and Other Microporous Solids*, Chap. 9, Wiley, New York (1992a).
Kärger, J., and D. Ruthven, *Diffusion in Zeolites and Other Microporous Solids*, Wiley, New York, p. 235 (1992b).
Kärger, J., and D. Ruthven, *Diffusion in Zeolites and Other Microporous Solids*, Wiley, New York, p. 393 (1992c).
Kočiřik, M., and A. Zikánová, "The Statistical Moments Method for the Calculation of the Coefficients of Radial Diffusion from Kinetic Measurements," *Z. Phys. Chem. Neue Folge*, **71**, 311 (1970).
Kocirik, M., and A. Zikánová, "The Analysis of the Adsorption Kinetics in Materials with Polydisperse Pore Structure," *Ind. Eng. Chem. Fund.*, **13**, 347 (1974).
Kondis, E. F., and J. S. Dranoff, "Kinetics of Isothermal Sorption of Ethane on 4A Molecular Sieve Pellets," *Ind. Eng. Chem. Process Des. Develop.*, **10**, 108 (1971).
Meier, W. M., and D. H. Olson, *Atlas of Zeolite Structure Types*, Butterworth-Heinemann, London (1992).
Micke, A., M. Bülow, and M. Kocirik, "A Nonequilibrium Surface Barrier for Sorption Kinetics of *p*-Ethyltoluene on ZSM-5 Molecular Sieves," *J. Phys. Chem.*, **98**, 924 (1994).
Nitsche, J. M., and J. Wei, "Window Effects in Zeolite Diffusion and Brownian Motion over Potential Barriers," *AIChE J.*, **37**, 661 (1991).
Reid, R. C., J. M. Prausnitz, and B. E. Poling, *The Properties of Gases and Liquids*, McGraw-Hill, New York (1987).
Riekert, L., "Transport of Mass and Heat in Porous Adsorbents," *Chem. Eng. Process.*, **26**, 59 (1989).
Ruckenstein, E., and P. S. Lee, "Resonant Diffusion," *Phys. Lett.*, **56A**, 423 (1976).
Ruthven, D. M., and K. F. Loughlin, "Correlation and Interpretation of Zeolitic Diffusion Coefficients," *Trans. Faraday Soc.*, **67**, 1661 (1971a).
Ruthven, D. M., and K. F. Loughlin, "The Sorption and Diffusion of n-butane in Linde 5A Sieve," *Chem. Eng. Sci.*, **26**, 1145 (1971b).
Ruthven, D. M., R. I. Derrah, and K. F. Loughlin, "Diffusion of Light Hydrocarbons in 5A Zeolite," *Can. J. Chem.*, **51**, 3514 (1973).
Ruthven, D. M., *Principles of Adsorption and Adsorption Processes*, Chap. 5, Wiley, New York (1984).
Ruthven, D. M., and M. Eic, "Intracrystalline Diffusion in Zeolites," *Perspectives in Molecular Sieve Science*, W. H. Flank and T. E. Whyte, eds., p. 362 (1988).
Vavlitis, A. P., D. M. Ruthven, and K. F. Loughlin, "Sorption of *N*-Pentane, *N*-Octane, and *N*-Decane in 5A Zeolite Crystals," *J. Coll. Interface Sci.*, **84**, 526 (1981).
Wei, P. B., "Zeolites—New Horizons in Catalysis," *Chemtech*, **3**, 498 (1973).
Xiao, J., and J. Wei, "Diffusion Mechanism of Hydrocarbons in Zeolites: I. Theory," *Chem. Eng. Sci.*, **47**, 1123 (1992).

Manuscript received Oct. 7, 1994, and revision June 13, 1995.